# Micro-Seismicity in the Southwestern Yukon, Canada

by

Lindsey Nicole Meighan

B.Sc.,York University, 2010

A Thesis Submitted in Partial Fulfillment
of the Requirements for the Degree of

MASTER OF SCIENCE

in the School of Earth and Ocean Sciences

# Supervisory Committee

Micro-Seismicity in the Southwest Yukon, Canada

by

Lindsey Nicole Meighan

B.Sc., York University, 2010

**Supervisory Committee**

Dr. John Cassidy, (School of Earth and Ocean Sciences; Geological Surveys of Canada Pacific, Natural Resource Canada)
**Co-Supervisor**

Dr. Stephane Mazzotti, (School of Earth and Ocean Sciences; Université Montpellier 2, France)
**Co-Supervisor**

Dr. George Spence, (School of Earth and Ocean Sciences)
**Departmental Member**

# Abstract

**Supervisory Committee**
Dr. John Cassidy, (School of Earth and Ocean Sciences; Geological Surveys of Canada Pacific, Natural Resource Canada)
**Co-Supervisor**
Dr. Stephane Mazzotti, (School of Earth and Ocean Sciences; Université Montpellier 2, France)
**Co-Supervisor**
Dr. George Spence, (School of Earth and Ocean Sciences)
**Departmental Member**

The objective of my research is to provide a better understanding of the relationship between the micro-seismicity, tectonics and crustal structure in southwest Yukon in order to improve seismic hazard assessments in this region. I used a combination of single event and multiple event location techniques to determine earthquake locations and depths. As well, frequency-magnitude statistics were calculated to analyze rates of seismicity and possible changes in the rates of seismicity.

The addition of the YUK array in August 2010 has enabled location of smaller events and detection of a systematic northeast trend of earthquakes. Seismicity is concentrated in four main areas: 1) Yaktutat Block-Fairweather Fault, 2) Duke River Fault, 3) Denali Fault, and 4) a NE-trend. There was relatively little seismic activity during this period along the northern Denali Fault segment and only a small amount of activity along the southern portion of the Denali Fault. There is significantly more seismic activity along the Duke River Fault and NE-trend and a clear region of seismicity just west and parallel to the Alaska-Yukon border between the Duke River Fault and northern Denali Fault. Frequency-magnitude statistics and seismic hazard analyses for southwest Yukon were improved by decreasing the minimum magnitude of completeness from M3.0 to M1.0.

Between September 2010 and November 2011, event magnitudes ranged from 0.2 to 4.7 and depths from 0 to 35 km.

To address how the YUK array has improved single event locations and depths, we use a single-event location technique to monitor seismic activity. Only 37 of the 106 events detected for the Duke River Fault and NE-trend could potentially be located without the YUK array. When the Alaska Earthquake Information Center (AEIC) network was combined with the Canadian National Seismograph Network (CNSN), events within the NE-trend shift on average 6.6 km to the northeast and the depth increased on average 2.6 km. Within the Duke River and NE-trending clusters, there is an average maximum horizontal error of ±0.9 km and an average error in depth of ±3.2 km.

Free depths in the Duke River and NE-trending clusters range from 0 to 20 km. These depths are not well-constrained as the closest station is more than 20 km away. Two events within the southern Denali Fault cluster have well-constrained depths of 4.8 km and 8.2 km at distance less than ~8 km from station YUK6, consistent with upper crust (2-10 km) focal depths.

A Progressive Multiple Event Location technique (PMEL) was used to identify and better constrain spatial patterns along the Duke River Fault and NE-trend. Results clearly shows that events fall along the Duke River Fault and that the NE-trend events are located on a previously unidentified active fault.

To determine rates of seismicity and possible changes in the rates of seismicity, I examine *b*-values from frequency-magnitude statistics for each cluster of earthquakes before and after the 2002 M7.9 Denali Fault earthquake. *b*-values increased from 0.81 ±

0.14 to 1.05 ± 0.22 , suggesting higher Coulomb stress and more frequent smaller earthquakes.

# Table of Contents

# List of Tables

# List of Figures

# Acknowledgments

Most importantly, I would like to thank my supervisors John Cassidy and Stephane Mazzotti for their guidance with my research and thesis writing. I would also like to thank my other committee member George Spence and external examiner John Clague for their helpful suggestions and corrections to my thesis.

A very special thanks to Gary Pavlis (Indiana University, Bloomington) and Roger Hansen (University of Alaska Fairbanks) who provided me with data from the Alaska Regional Network and guidance with the Progressive Multiple Event Location (PMEL) results in my thesis. Also special thanks to Taimi Mulder (Geological Surveys Pacific) for her continuous guidance using ANTELOPE software for earthquake locations.

Thank you to my mother and father for their endless support and encouragement.

# Chapter 1: Introduction

## 1.1 Objectives

The northern Canadian Cordillera is one of the most tectonically and seismically active areas of Canada. One of the challenges in studying the seismic hazard of this region in detail is the paucity of data. For example prior to 2010, only three permanent seismic stations were installed in Yukon Canada.

In the summer of 2010, a new dense seismic array (YUK) was deployed in southwest Yukon. This array enables detection of micro-seismicity in the region, with more accurate earthquake location and depths. The objective of this thesis is to provide a better understanding of the relationship between the micro-seismicity and the tectonics and crustal structure of southwest Yukon in order to improve seismic hazard assessments in the region. This will be addressed by focusing on the following three points:

1. Improve earthquake location and depth estimates in southwest Yukon using the new YUK array.
2. Identify and constrain spatial patterns of earthquakes using a precise location technique (Progressive Multiple Event Locations, PMEL)
3. Evaluate rates of seismicity and possible changes in rates of seismicity.

The new YUK array will better constrain spatial micro-seismicity patterns in the crust, identify active structures and the corresponding frequency-magnitude statistics. Improved micro-seismicity patterns and frequency-magnitude statistics will help to improve our understanding of the source of earthquake hazard in the Yukon. There have been several

large historical earthquakes (M>7) in the vicinity of southwest Yukon over the last century, and with the development of the Alaska Pipeline Project (TransCanada, 2012) there is a great need to better characterize seismic hazard in this region.

## 1.2 Tectonic Setting and Seismicity of the Northern Canadian Cordillera

The Cordillera can be divided into four main tectonic domains, from the south to north (Figure 1): the Cascadia subduction zone; the Queen Charlotte-Fairweather transform region; the Yakutat collision zone; and the Alaska-Aleutian subduction zone (Mazzotti et al., 2008). The Cordillera can also be divided into four geological belts: the northerly east-west-trending Arctic Alaska; central southwest-trending Ruby; southerly east-trending Dllinger; and southeast-trending Yukon-Tanana belts (Johnston, 2001). These belts are characterized by four regularly arranged rock sequences: a Paleozoic continental margin strata; a Devonian-Mississippian arc assemblage; an ophiolitel; and an early to mid-Cretaceous arc (Johnston, 2001).

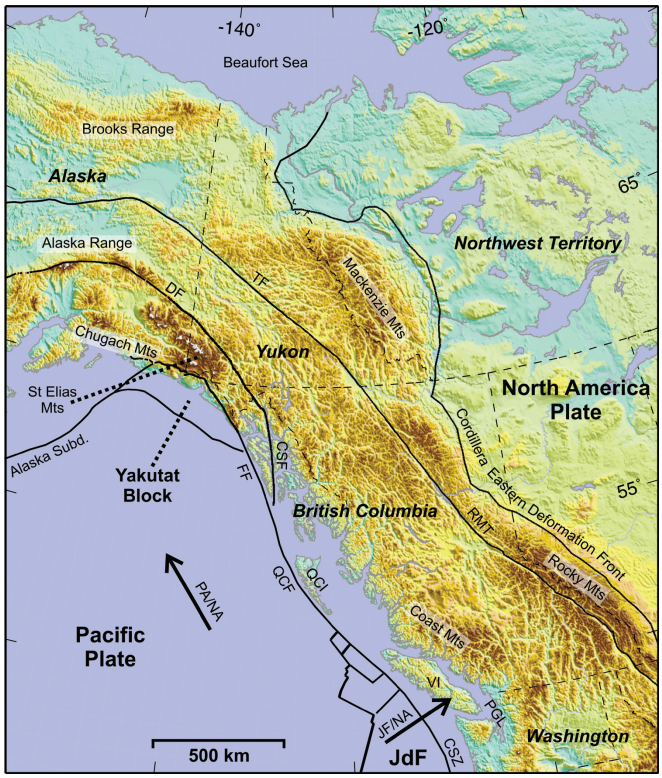


**Figure 1: Topography and tectonic framework of the Northern Cordillera. Beaufort Sea; Brooks Range; Mackenzie Mountains; TF, Tintina Fault; DF, Denali Fault; St. Elias Mountains; Chugach Mountains; FF, Fairweather Fault (Mazzotti et al., 2008).**

The northernmost Canadian Cordillera is a tectonically and seismically active area that is moving inland to the northeast at a rate of 5 mm/yr relative to the North American craton, based on GPS velocities (Hyndman et al., 2005). This region represents a transition from strike-slip tectonics in the south to collision tectonics in the Yakutat region. The consistent plunge of structures across southwest Yukon suggests the crust has been uniformly tilted to the east-southeast, where deep structural levels of the crust are exposed to the west and shallower levels to the east (Johnston & Canil, 2007).

Rapid uplift, crustal thickening and high seismicity in the neighbouring St. Elias and Chugach Mountains are primarily due to the collision of the Yakutat Block, a small oceanic-continental terrane in the Gulf of Alaska, which is moving northwestward, with the Pacific plate along the North America western margin (Hyndman et al., 2005). The collision of the Yakutat Block is inferred to cause strong seismicity 600-800 km northeast of the collision zone in the Mackenzie and Richardson Mountains of the Northern Cordillera Foreland Belt (Leonard et al., 2008). Major fault systems include the Denali, Tintinia, Fairweather, Queen Charlotte, Chugach-St. Elias, Pamplona, Chatham Strait and Transition Faults (Figure 2). In this thesis I focus on seismicity in the vicinity of Denali Fault and Duke River Fault.

The Denali Fault system has accommodated about 400 km dextral displacement over the past 55 Myr. Focal mechanisms indicate that current activity on the Denali Fault is mostly dextral strike-slip. The southern portion of the Denali Fault indicates a deformation rate of 2.0 mm/yr right lateral motion based on the seismic moment, shear modulus and fault rupture area (Leonard et al., 2008). Previously, seismicity has been too sparse to determine deformation rates for the northern part of the Denali Fault. The Duke River Fault has 3.1 mm/yr right lateral slip and 1.5 mm/yr compressive movement based on relative block motions (Leonard et al., 2008).

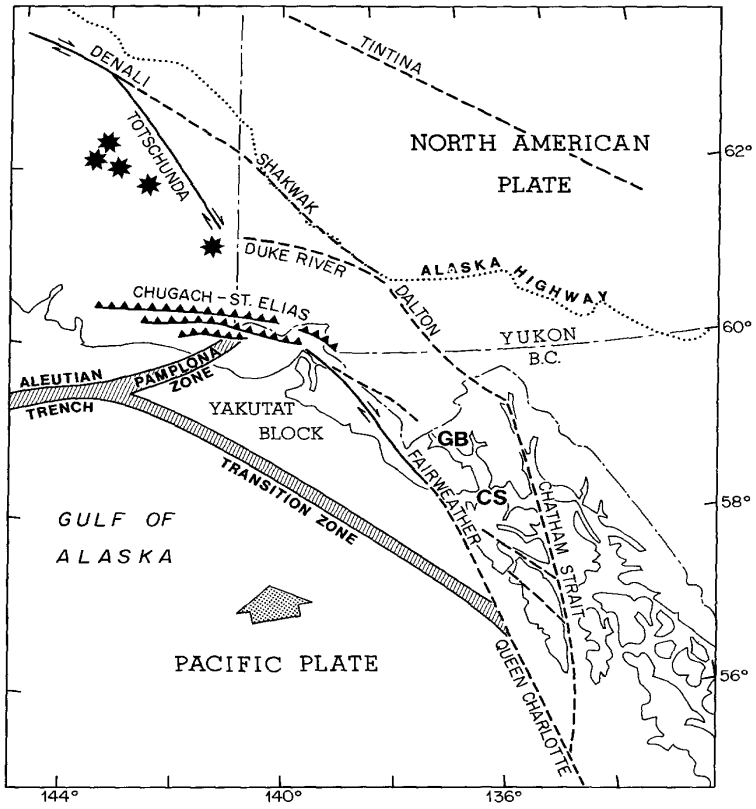


**Figure 2: Major tectonic elements in the St. Elias region after Platker et al. (1978). Stars denote volcanoes of Quaternary age. Relative motion between Pacific and American plates indicated by arrow. Most of the convergence is accommodated by predominantly strike-slip faulting on the Queen Charlotte- Fairweather Fault and thrust faulting along the Pamplona zone extending into the Aleutian megathrust. Dashed fault lines on land indicate those with no geologic evidence for Holocene displacement. Other symbols are: GB, Glacier Bay and CS, Cross Sound (Horner, 1983).**

### 1.2.1 Seismicity and Earthquake Monitoring

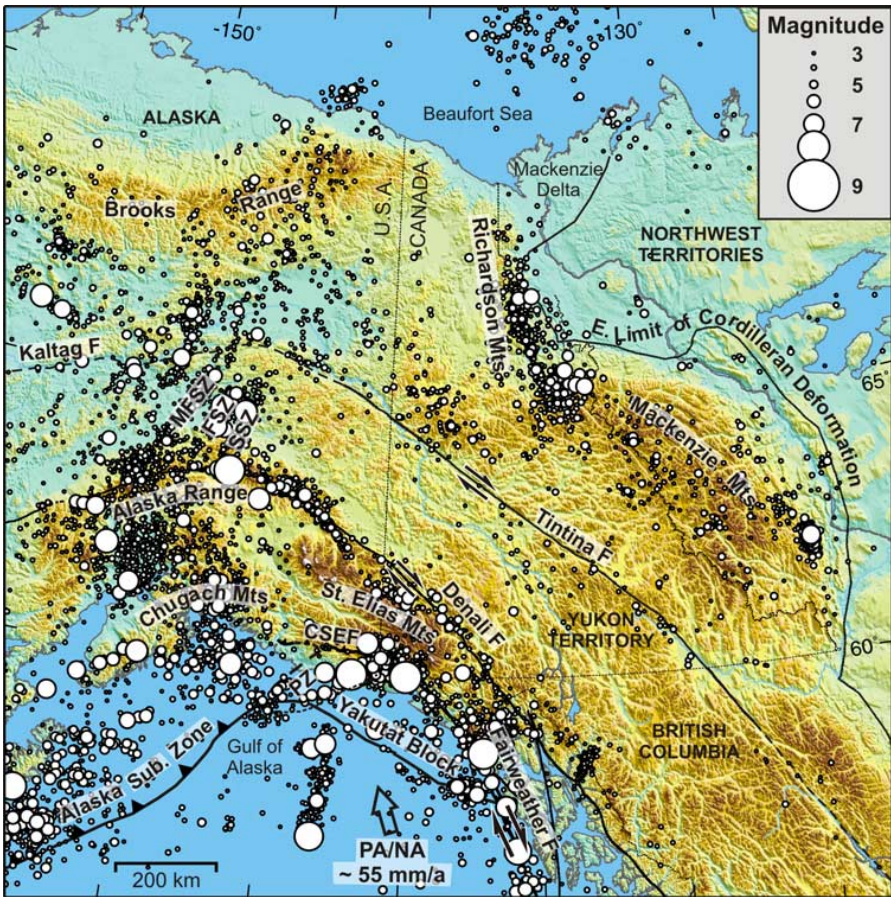


**Figure 3: Seismicity of the northern Canadian Cordillera of Canada and eastern Alaska. White circles are earthquakes M ≥ 3, 1899–2004. Data are from the Geological Survey of Canada National Earthquake Database and the Alaska Earthquake Information Centre Database (2005) (Leonard et al., 2008).**

Prior to 2010 earthquake locations in the northern Canadian Cordillera were based only on three permanent stations (DAWY, HYT, WHY), shown in Figure 4. For earthquakes after 1971 but prior to the establishment prior to the YUK array, locations had relatively large horizontal location errors (±5-10 km) and focal depths were not routinely determined (Leonard et al., 2008).

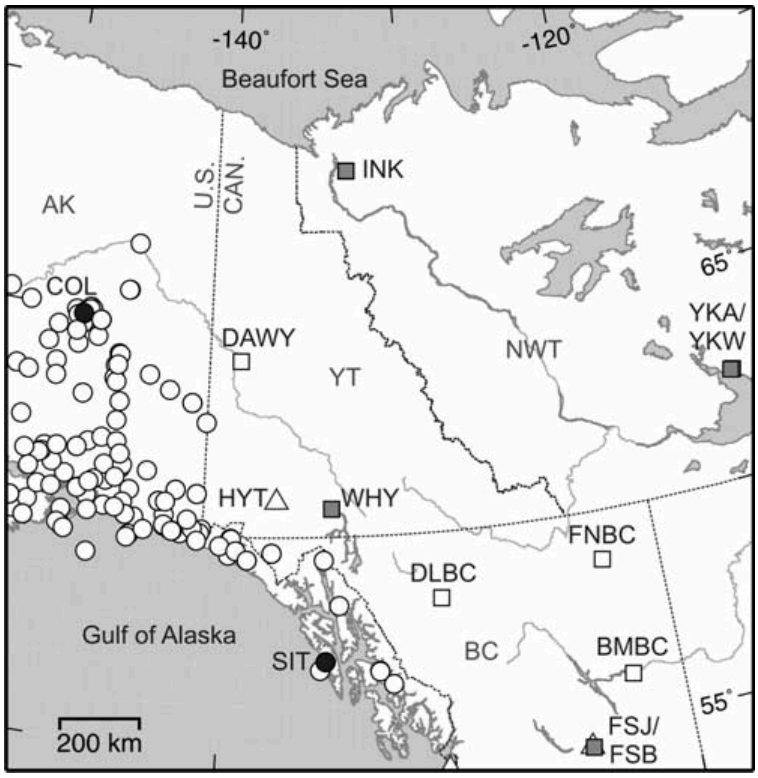


**Figure 4: The seismic network in the northern Canadian Cordillera in 2004. Squares show three-component broadband stations of the Canadian National Seismograph Network (CNSN); triangles represent single-component short-period stations of CNSN, circles represent Alaska seismic stations (Leonard et al., 2008).**

Most earthquakes (and the largest ones) occur in the region along the plate boundary in the coastal and offshore area. Some of the most significant earthquakes include: 1899 sequence of events (M7.8, 8.2 and 8.6) at the Yakutat Bay, 1958 M7.6 event on the Fairweather fault, 1972 M7.6 event along the northern end of the Queen Charlotte fault, 1979 M7.5 event along the Chugach-St. Elias fault, the 1920 M6 event near the Denali Fault in the Yukon, the 1952 M6 event near the northern end of the Fairweather fault and the 2002 M7.9 Denali Fault earthquake in Alaska (Cassidy et al., 2005).

The most significant inland seismicity in the northern Cordillera is along the Denali Fault. The largest earthquake to occur in the vicinity of the Canadian portion of the

Denali Fault is a $M_s$6.5 event in 1944 (Cassidy et al., 2005). In 2002, a $M_w$7.9 earthquake occurred on the Alaska portion of the Denali Fault. There is relatively little seismic activity between the Denali Fault and Tintina Fault. Only small earthquakes (M<3.0) have been observed on the Tintina Fault (Cassidy et al,. 2005).

Rates of seismicity for a M>5 earthquake in Yukon are approximately one earthquake every 1.5 years along the coast, one every 3-5 years in the vicinity of the Denali Fault and one every 30 years in the Yukon interior (Cassidy et al., 2005). Significant earthquakes in the northern Cordillera typically occur in pairs or sequences, suggesting that the Coulomb stress changes has an influence on seismicity in this region (Cassidy et al., 2005).

### 1.2.2 Yakutat Block

The Yakutat Block is a small oceanic-continental terrane that has been colliding obliquely with the continent in the Gulf of Alaska since the Miocene. It is currently moving with the Pacific plate but slightly slower and in a more westward direction. The block is being forced to the west around the Gulf of Alaska along a series of strike-slip and thrust faults, and a smaller component of motion is transferred inland to the northeast across the Cordillera at a rate of 5 mm/yr (Hyndman et al., 2005). The block has thick Cretaceous continental crust margin in the east (Chugach terrane) and Paleogene oceanic crust in the northwest. Both parts are overlain by Cenozoic sedimentary rocks (Hyndman et al., 2005). The Yakutat terrane is bounded to the east by the transcurrent Fairweather Fault and to the southwest by a transpressive right-lateral strike-slip fault called the Transition Fault System (Figure 5). To the north, the Yakutat Block experiences underthrusting and accretion mainly along the St.Elias-Chugach Fault system (Mazzotti

& Hyndman, 2002). GPS data show that, relative to the North America plate, the Yakutat Block is moving 44-47 mm/yr toward N 22-29° W (Leonard et al., 2008). Figure 5 illustrates Yakutat collision zone seismicity.

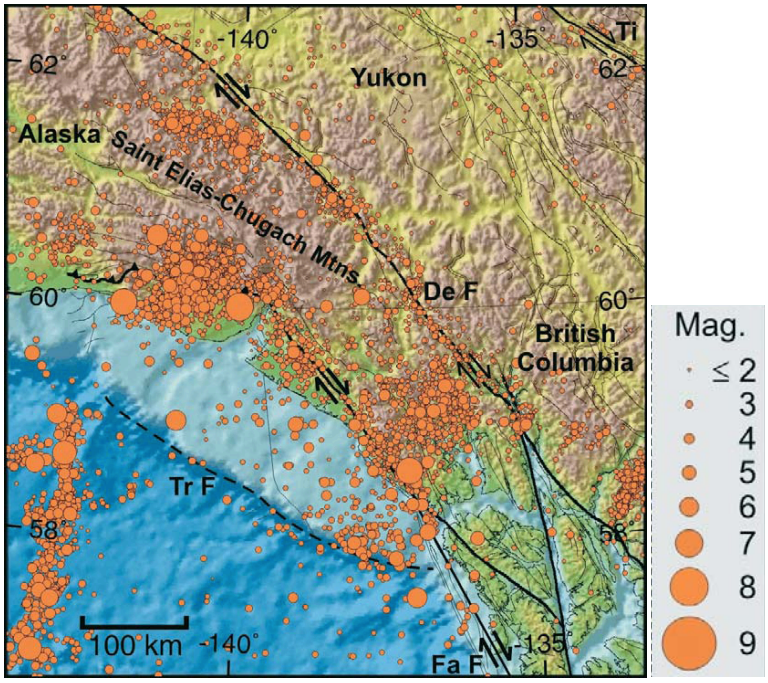


**Figure 5: Detail of Yakutat collision zone seismicity. Fa F, Fairweather Fault; Tr F, Transition Fault (Hyndman et al., 2005).**

### 1.2.3 Saint Elias and Chugach Mountains

The Chugach terrane is an accretionary complex formed by convergence and underthrusting of the Yakutat terrane from the latest Triassic to earliest Tertiary time (Hyndman et al., 2005). Convergence and underthrusting of the Yakutat Block beneath the Chugach terrane produced a fold-and-thrust belt along the Saint Elias-Chugach Fault system about 20 Ma ago and andesitic volcanism in the Wrangell Mountains. This

transpression caused rapid uplift and crustal thickening in the Chugach and St. Elias Mountians, creating Canada's highest peak, Mount Logan (Hyndman et al., 2005).

### 1.2.4 Richardson and Mackenzie Mountains

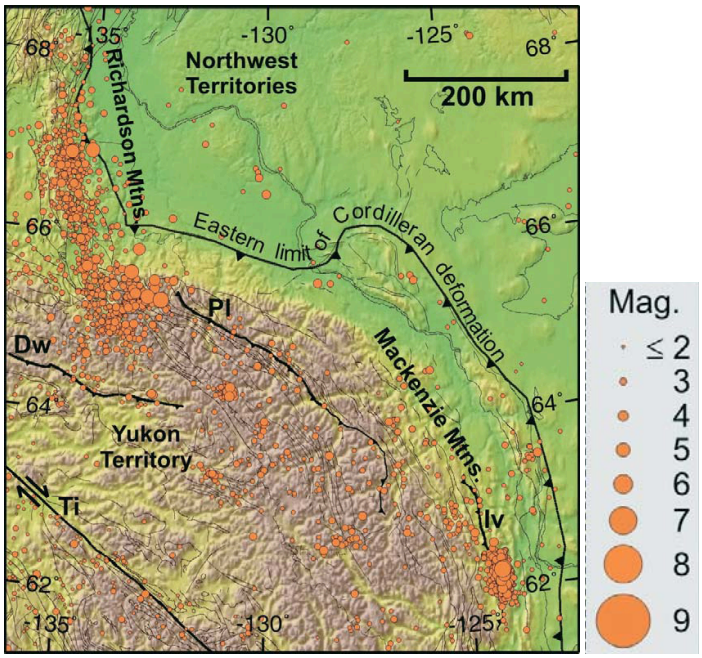


**Figure 6: Seismicity in Yukon east of the St. Elias Mountains. Dw, Dawson thrust; Iv, Iverson thrust; Plateau thrust; Ti, Tintina fault. (Hyndman et al., 2005)**

The Mackenzie and Richardson Mountains display two types of tectonic styles. Regional geology suggest mainly contractional fold and thrust faults in the Mackenzie Mountains and right lateral strike-slip faults in the Richardson Mountains (Figure 6).

Studies of earthquake depth distribution indicate a seismic crustal thickness or maximum depth of seismicity of 10-15 km in the Mackenzie and Richardson mountains. The maximum magnitude for a region is important for determining deformation rates from seismicity (Figure 7). The maximum magnitude earthquake in each area is determined using the length of the largest fault, the seismic thickness, and an empirical

relation between magnitude and fault area. Based on the maximum magnitudes, there is a shortening rate in the Mackenzie Mountains of 4.5 ± 2.5 mm/yr, and a right-lateral strike-slip rate in the Richardson Mountains of 5 ± 2.5 mm/yr (Mazzotti & Hyndman, 2002). The uncertainties are based on statistical errors, seismic thickness and maximum magnitude.

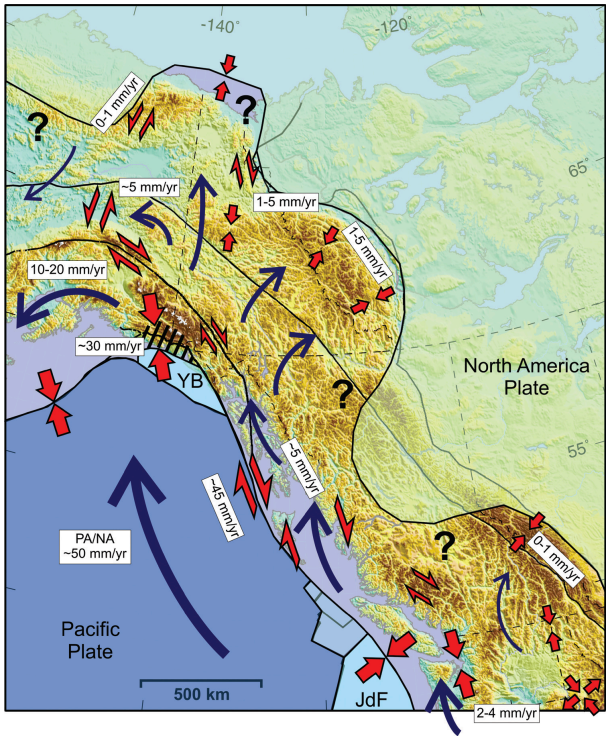


**Figure 7: Active tectonics of the northern Cordillera. The tectonic model is derived from GPS data, earthquake statistics, and focal mechanisms. The curved blue arrows show motion of the Pacific Plate (blue shade) and Cordillera internal blocks and deforming areas with respect to the North American plate (green shade). Red arrows indicate areas of shortening and strike-slip deformation. The areas marked by black diagonal lines represent the Yakutat collision zone. JdF is Juan de Fuca plate and YB is Yakutat Block (Mazzotti et al., 2008).**

## 1.3 Motivation

The southwest Yukon is a highly seismically active region with some of the highest mountains in Canada and highest peaks in North America. There have been many large historical earthquakes in the region. The 2002 M7.9 Denali Fault strike-slip earthquake ruptured 340 km of crust to near the Yukon-Alaska border with displacements of up to 8.8 m. Over a large area there was significant co-seismic and post-seismic deformation (Ruppert, 2008). The Fairweather Fault has ruptured in a series of mainly dextral strike-slip earthquakes in 1927, 1949,1958, and 1972. Due to the low population and limited infrastructure this region has not been studied in detail until the last ~50 years.

TransCanada and ExxonMobil began working together in 2009 to develop the Alaska Pipeline Project. The objective of the project is to connect Alaska's North Slope natural gas resources to new markets and deliver a reliable and secure source of clean energy. There will be many benefits to Alaska and the rest of the United States and Canada in terms of jobs, government revenues, business opportunities and long-term supplies of natural gas (TransCanada, 2012). There are two routes that are being considered (Figure 8). In the case of the proposed Alberta route, the pipeline would start Prudhoe Bay, Alaska, through southwest Yukon, and northern British Columbia and end north of Calgary, Alberta. The Alberta route has a total length of 2762 km, 1564 km in Canada and 1198 km in Alaska. The pipeline will pass through Beaver Creek, Burwash Landing, Destruction Bay, Haines Junction and Whitehorse in southwest Yukon. Improving earthquake epicentre locations and depth estimates in order to identify active structures in southwest Yukon and the potential for large earthquakes is an important consideration for infrastructure engineering and route planning. Importance of infrastructure engineering

and route planning was demonstrated during the 2002 M7.9 Denali Fault earthquake. There was an offset of the Richardson Hwy by up to 7 m and the Alyeska pipeline remained intact during 5.8 m of slip.

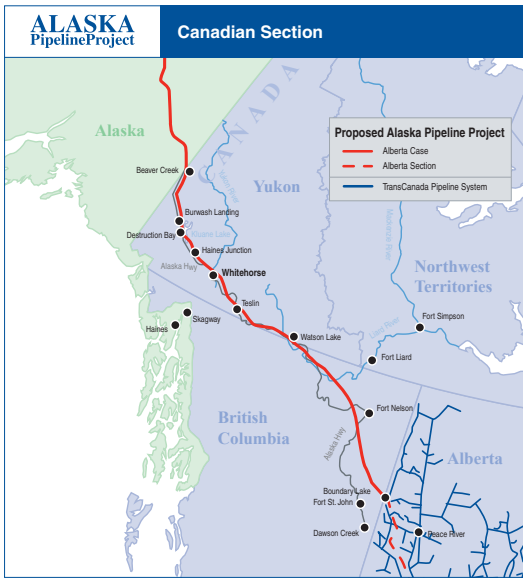


**Figure 8: Proposed route of Canadian section of the Alaska pipeline project. Black dots represent locations of compressor stations (TransCanada, 2012).**

# Chapter 2: Methods

This chapter discusses the procedure and techniques used to determine earthquake epicentre locations and depths, to calculate earthquake recurrence relations, and to identify active structures, all of which help to further our understanding of the source of seismic hazard in the region.

## 2.1 Single Event Locations

Standard earthquake locations use a single event location algorithm that creates a catalogue of travel times for each seismic network. This involves measuring the arrival times of seismic waveforms, called phase picks, and calculating the travel times based on a standard travel-time model. The first arriving P-wave, vertical component, and S-wave, horizontal component are picked by the technician. With the observed travel time, $t$, and a specified velocity, $v$, the distance between the hypocenter of the earthquake and seismic station can be calculated. Currently, a one-dimensional velocity model is used. With three or more seismic stations a least squares adjustment is used to minimize the difference between the observed and modeled travel times (Wood, 2010).

There are three sources of uncertainty in event locations:

1) Poor station coverage/geometry. With a sparse set of stations, locations can be in error by several tens of kilometres and depths are not constrained. A high station density (i.e. station separation of 10-20 km) and a good geometry of stations around an earthquake with at least one station at a relatively close distance (i.e. for depths of 10 km, a minimum station distance within 10 km) provides accurate locations and focal depths.

2) Difficulty picking arrival times accurately. Typically there is a picking error of 0.25 sec for P arrivals and 0.5 sec for S arrivals. Based on Monte Carlo analysis, a picking error of 0.25 sec will result in errors of less than ~5 km in epicentre location, 6 km in depth and 0.75 sec in origin time (Billings et al., 1994).

3) Errors in the travel-time model (velocity model) used to interpret measured arrival times. Often it is the model error that dominates the overall error in absolute locations. Thus, improving the travel-time model for absolute locations will result in substantial improvement in single event locations (Richards et al., 2006).

The precision defines the location uncertainty that leads to scatter of earthquake locations, typically caused by measurement errors of seismic arrival times and poor station geometry, whereas the accuracy defines the absolute location uncertainty due to systematic biases such as errors in station parameters (location, timing), errors in the velocity model, and misidentification of seismic phases (ie P, S, Pn, Sn etc) (Husen & Hardebeck, 2010).

### 2.1.2 Catalogue Arrival Times and Velocity Model

The catalogue arrival times were picked using the digital seismic analysis code *dbpick*, which is a component of the Antelope software system http://www.brtt.com/software.html. Antelope is a real-time system software comprising a collection of programs for data collection and seismic data analysis. Single event locations are processed using *dbloc2*, an interactive hypocenter location program that gives the location of hypocenters from previously picked trace data and has the ability to edit arrival picks. *dbloc2* is an interface program of *dbgenloc* (GENeric/GENeralized

LOCation) library that computes event locations using travel time and/or slowness measurements. The main database output tables are *origin*, *assoc* and *origerr*. The *origin* table gives the locations of each event in the catalogue; the *assoc* table associates arrivals with the origins in other catalogues; and the *origerr* table associates the errors of each location with the origin table. A generic one-dimensional layer over a half-space velocity model is used for the locations in this region, specified as model 1 in *dbloc2* (Table 1; Quinlan & Pavlis, 2007).

**Table 1: Velocity model 1 for northern Canadian Cordillera**

| VP (m/s) | Depth of top layer (km) | VS (m/s) |
|---|---|---|
| 6.2 | 0.0 | 3.57 |
| 8.2 | 36 | 4.70 |

## 2.2 Progressive Multiple Event Locations (PMEL)

To identify and better constrain spatial patterns within seismically active regions, a multiple event location method was used to refine relative hypocenter locations. This method is commonly used to identify active structures. PMEL is a location algorithm that gathers hypocenters in close spatial proximity to one another (Hamburger et al., 2011). PMEL uses the *genloc* library as a foundation. *dbpmel* is an updated database implementation of PMEL (Pavlis & Booker, 1983) that was designed to locate events of entire catalogues but can also be used to locate mainshock-aftershock sequences.

The term progressive is used to distinguish this method from other relocation techniques, in particular from that of Joint Hypocenter Decomposition (JHD). JHD

adjusts all unknown parameters in one large matrix inversion using normal equations, whereas *dbpmel* performs a series of iterative adjustments in a fixed sequence to the unknown parameters using orthogonal transformations, resulting in a more numerically stable algorithm. In contrast to some other relocation techniques, *dbpmel* does not require a master event at each station and also reduces errors in the station corrections. The hypocentroid, or centre of mass of the cluster, acts like a pseudo-master event (Pavlis & Booker, 1983).

In general, multiple event location methods will assume that errors in the travel-time model (velocity model) are absorbed into a set of time constants, called station corrections. However, *dbpmel* determines an exact solution to this problem by solving a matrix where the given data are the observed arrival times of an ensemble of events and the unknowns are: 1) the location of the events within the ensemble and 2) a set of station corrections. Travel-time model errors are only effective for a limited area in space, thus *dbpmel* locates an entire catalogue by gathering events into ensembles based on spatial position. The groups of events is defined by a table called "cluster" that is linked to a particular point in space or an associated grid point. *dbpmel* locates each "cluster" of events associated with a grid point and estimates a set of station corrections for each grid point (Pavlis, 2008). Hypocenter locations are estimated individually and their residuals are accumulated to estimate station corrections. Because earthquake locations are adjusted iteratively after each station correction adjustment, *dbpmel* promotes rapid convergence of the unweighted raw residual misfit.

When using *dbpmel,* there is an increase in event origins because one event may fall into several clusters, raising an issue of redundancy in event locations. To estimate this

redundancy in arrival time estimates, we take an average to produce one arrival time for each event and thus produce one event location. Locations with a significantly different root mean square (rms) compared to the other events within the cluster are considered outliers. The error scale used to define outliers is not determined independently for each event as it is for single locations using *dbgenloc*, but rather is based on the global rms of each cluster of events.

Often before running a relocation algorithm, the analyst uses waveform cross-correlation to ensure that the P and S wave arrival times are picked at exactly the same phase at all stations. This strategy ensures the errors in arrival time picks will not affect the precision of the relative locations. Since cross-correlation consistently aligns the main pulses, there is less scatter in the travel time residuals and final relative event locations. Cross-correlation was attempted using source side array processing, called *dbxcor*. It uses an iterative stacking algorithm to align all data by cross-correlation and to create an array stack for each ensemble. The stack is determined by a robust weighting scheme to decrease the value of data that differ strongly from the stack. The stack changes iteratively, allowing changes in weight and time to each waveform trace until all time-shift changes below a chosen master trace in the stack of waveforms become small. The user selects a master reference trace and then removes waveforms that are below a chosen threshold cross-correlation coefficient due to a poor signal-to-noise ratio or a poor match to the reference trace. This process can be repeated, selecting different master reference traces each time. Thus, the dataset can give completely revised arrival times and identify all correlations between waveforms. *dbxcor's* main advantage is that arrival estimates are reviewed iteratively by the user, unlike other automated processing cross-correlation

algorithms. I decided, after assessing the waveforms at YUK2 and YUK3, that there were not enough similarities between waveforms to properly take advantage of *dbxcor*. However, in such a case, *dbxcor* can still be used to edit arrival time picks.

## 2.3 Gutenberg-Richter Relation

The Gutenberg-Richter relation is a well-defined empirical relation in seismology that represents the frequency of earthquakes as a function of magnitude and describes the relative occurrence of large and small events:

$$\log_{10}N = a - bM$$

where M is the minimum magnitude of earthquakes for N cumulative number of earthquakes, and *a* and *b* are constants (Gutenberg & Richter, 1944). The magnitude-frequency distribution is a power law distribution, where the *b*-value represents the slope of the log-linear distribution or earthquake size distribution, and the *a*-value represents seismicity rate or productivity (Gutenberg & Richter, 1944). Higher *b*-values describe a greater frequency of smaller earthquakes, whereas a lower *b*-value describes conditions for less frequent but moderate to large earthquakes (Wiemer & Wyss, 2002). The global average *b*-value is about 1, and typically values range between 0.6 and 1.4. Volcanic areas may have *b*-values as high as 3.0. The main factors that may control differences in *b*-values are high and low ambient stresses, material heterogeneity, and thermal gradients. *b*-values less than 1 indicate crustal homogeneity and higher ambient stress (lower pore pressure), whereas values greater than 1 indicate crustal heterogeneity and lower ambient

stress (higher pore pressure) (Bridges & Gao, 2006). There are four assumptions on which the Gutenberg-Richter calculations are based (Main et al., 1999):

1) There exists a finite maximum magnitude.

2) Earthquake recurrence is statistically stationary. The event rate and mean magnitude do not change with time.

3) The region is homogenous. There are no major areas with characteristics significantly different within expected statistical fluctuations.

4) The log-linear relationship of the incremental frequency is true for all magnitude values (i.e. equation 1 holds for all for all magnitudes below $M_{max}$).

When using the Gutenberg-Richter relation, we assume self-similarity of earthquake occurrence, which implies that earthquake properties should scale uniformly from small to large magnitudes (Rydelek & Sacks, 1989). However, some studies have shown that there is a break in similarity between small and large events; small earthquakes tend to scale differently with rupture length than large earthquakes. Deviation in linearity may be biased by small earthquakes because of the limited number of events of large magnitude or due to magnitude incompleteness, or an incorrect minimum magnitude detection threshold (Pacheco et al., 1992).

Although we assume homogeneous conditions using the Gutenberg-Richter relation, spatial heterogeneity in seismicity parameters has been well established. Seismicity rates or productivity (*a*-value) and earthquake size distribution (*b*-value) both strongly vary in space and to a lesser degree in time. In the case where these parameters temporally change (non-stationary), large sample sizes may average out fluctuations for a better long-term forecast; however large sample sizes do not account for spatial heterogeneity.

A smaller sample size has higher resolution and takes heterogeneity into account, but increases the uncertainty of estimating model parameters. Thus there is a trade-off between accuracy and resolution of the data. Based on the Gutenberg-Richter law, a temporally homogenous seismic catalogue with roughly 50-100 events is required to calculate and map accurate *b*-values (Schorlemmer et al,. 2004).

In this study, frequency-magnitude distributions have been calculated using Stephane Mazzotti's 2001-2002 Fortran code (Geological Survey of Canada (GSC) Pacific of Natural Resource Canada (NRCan)). The Fortran code provides an estimate of the frequency-magnitude distribution and moment release/deformation rate from a catalogue of earthquakes with different completeness periods using a maximum likelihood estimation (Weichert, 1980). The frequency-magnitude distribution is calculated, the incremental and cumulative distributions are plotted over a chosen magnitude range, and a fitted truncated Gutenberg-Richter (GR) curve is generated:

$$N(M) = T\frac{e^{-\beta M} - e^{-\beta m}}{1 - e^{-\beta m}}$$

where N is the number of earthquakes with magnitudes equal or greater than M, T is the total number of earthquakes with non-negative magnitudes, m is a constant and $\beta \cong 2.3b$ (Cornell & Vanmarcke, 1969).

The Fortran code for estimating the frequency-magnitude distribution requires an input file that asks for an earthquake data file, catalogue completeness table, the last complete year of data in the earthquake file, and the minimum and maximum magnitude. The catalogue completeness table represents complete earthquake detection and differs from

region to region. With improvements in the station coverage, the lower limit of complete earthquake detection has decreased over time. The GSC completeness intervals are used as a starting point, with some adjustments based on the magnitude distribution over time (Table 2).

**Table 2: Magnitude intervals of completeness used for each region (Leonard et al., 2008).**

| 1850 | 1899 | 1917 | 1935 | 1951 | 1961 | 1965 | 1972 | 1979 | 2011 |
|---|---|---|---|---|---|---|---|---|---|
| 7.3 | 7.2 | 6.3 | 5.8 | 5.3 | 4.8 | 4.3 | 3.8 | 3.0 | 1.0 |

The minimum and maximum magnitudes for each cluster were determined separately. The minimum magnitude cutoff ($M_{min}$) occurs approximately where frequencies start to fall below the linear Gutenberg-Richter curve, that is any magnitude less than the Gutenberg-Richter distribution. Any magnitude below the minimum magnitude cutoff is considered incomplete. The minimum magnitude for each time interval and region is mainly controlled by the completeness catalogue in Table 2. Minimum magnitude cutoff ($M_{min}$) is chosen so that the parameters *a* and *b* are stable values and should be higher than the minimum magnitude of the completeness tables.

Before the new YUK array was installed, the minimum magnitude of the completeness table for the Duke River and Denali Faults was 3.2 (Leonard et al., 2008). With the new YUK array, $M_{min}$ of the completeness table is about 1.0 for all regions in southwest Yukon. Smaller magnitudes are detectable around the Duke River Fault with the greater concentration of stations compared to the northern and southern segments of the Denali Fault.

The maximum magnitude ($M_{max}$) was chosen based on the largest earthquake possible in the area of interest. There is no significant change in *b*-value if a reasonable maximum magnitude is chosen. A $M_{max}$ that is too low will result in a significantly lower *b*-value. Studies have shown that earthquake magnitude is related to rupture parameters; surface rupture length is known to be strongly correlated to earthquake magnitude (Wells & Coppersmith, 1994). The strong correlation between rupture parameters and magnitude allows us to estimate magnitudes or rupture parameters for different areas of interest. For example, the Duke River Fault has a maximum magnitude of 7.6. *b*-values will remain relatively constant when an appropriate $M_{max}$ of ± 1 magnitude unit is chosen. The uncertainty in $M_{max}$ depends mainly on the availability and reliability of constraining data, which differs from region to region (Leonard et al., 2008). Empirical regressions between magnitude and surface rupture length, and subsurface rupture length, downdip rupture width and rupture area have correlation coefficients of about 0.84 and 0.95 and standard deviations of about 0.24 and 0.41 magnitude units (Wells & Coppersmith, 1994).

## 2.4 Frequency-Magnitude Relation and Coulomb Stress Changes

A fault may consist of locked segments that resist slipping (asperities), unlocked segments described by creep and segments with intermediate properties. In locked segments stresses are concentrated and build up, whereas unlocked segments stresses are relieved and do not build up. Mainshock events typically originate from asperities. When a fault ruptures, it may only involve one asperity and result in a large earthquake, or it may involve many neighboring asperities and continue to generate a larger earthquake. Thus, we can expect variations in *a* and *b*-values for different fault segments due to fault properties and stress variations. Low *b*-values are related to a strong and homogenous stress field near an asperity. Creeping segments tend to have high *b*-values and thus are more conducive to triggering smaller earthquakes (Wiemer & Wyss, 2002).

It has been suggested that recurrence time of mainshocks are determined by the process operating around the asperity (Wiemer & Wyss, 2002) . If variations in stress due to a large earthquake cause changes in *a* and/or *b*-values, there will be changes in the local reoccurrence time and probability (Wiemer & Wyss, 2002).

There is evidence that *b*-values are different before and after a mainshock (Wyss & Wiemer, 2000). A change in the probability of future earthquakes in the vicinity of a mainshock is due to changes in the Coulomb failure criterion. The Coulomb failure criterion requires that both the normal and shear stress on a fault plane satisfy conditions comparable to those of friction on a pre-existing fault surface. Failure occurs on a fault plane when the Coulomb stress exceeds a specific value:

$$\Delta\sigma_f = \Delta\tau + \mu^*(\Delta P + \Delta\sigma_n)$$

where $\Delta\sigma_f$ is the Coulomb stress, $\Delta\tau$ is the shear stress, $\Delta\sigma_n$ is the normal stress, $\mu$ is coefficient of friction and $\Delta P$ is the pore fluid pressure. Failure is more likely for positive Coulomb stress values and less likely for negative values. Studies suggest that an increase of Coulomb stress of less than 1 bar is enough to trigger events, whereas the same decrease is enough to suppress them (Wiemer & Wyss, 2002). Higher shear stress will promote additional earthquakes.

# Chapter 3: Data

The YUK array was deployed in the summer of 2010 to investigate micro-seismicity in southwest Yukon in order to better constrain earthquake locations and depths and corresponding frequency-magnitude statistics. Data consist of earthquakes located within the region of 58° to 62° N and -142° to -134° W from September 2010 to November 2011. In the region there were 980 events located during this period. Here I focus on four clusters of earthquakes consisting of 169 events: the Duke River Fault, the NE-trend, and the northern and southern Denali Fault segments (Figure 9). Duke River Fault cluster consists of 54 events, the NE-trend 68 events, northern Denali Fault 11 events, and southern Denali Fault 36 events. Magnitudes range from 0 to 3.0. For frequency-magnitude statistics I expanded the dataset to include earthquakes located from 1985 to the end of 2011.

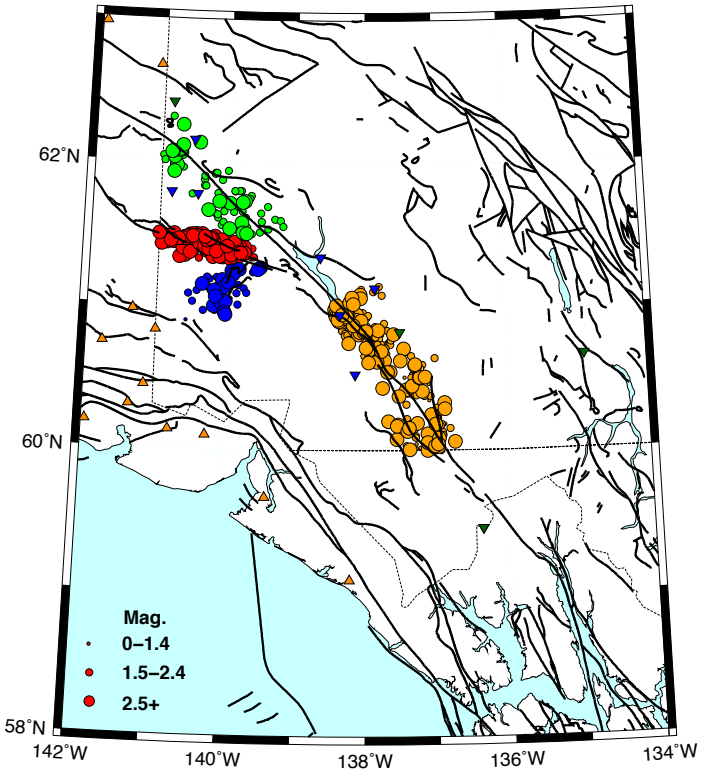


**Figure 9: Four clusters of earthquake located between 1985 and 2011. Blue circles are the NE-trend; orange circles are the southern Denali Fault cluster; red circles are the Duke River Fault cluster; and green circles are the northern Denali Fault cluster.**

## 3.1 Networks

Earthquake locations in southwest Yukon are based on a combination of Canadian and United States seismic stations. The Canadian National Seismograph Network (CNSN) is the primary earthquake catalogue used for the single and multiple event locations and frequency-magnitude statistics. The new array (YUK 1-7), installed in the summer of 2010 consists of high broadband (short period frequencies) CNSN stations (100 sps: HHZ/N/E). The original Canadian network of high broadband stations include stations: PLBC, HYT, WHY, BVCY, and DAWY.

The Alaska Regional Seismic Network of the Alaska Earthquake Information Center (AEIC) records and analyzes data from several networks in Alaska and surrounding areas. A new, 24-station seismic network was installed during the St. Elias Erosion and Tectonics Project (STEEP) in 2005 and 2006. The STEEP network and several stations of AEIC are included with the CNSN network to further improve the accuracy and depth estimates of the standard earthquake locations. Figure 10 shows the locations of the CNSN and Alaska stations considered for the single and multiple event locations.

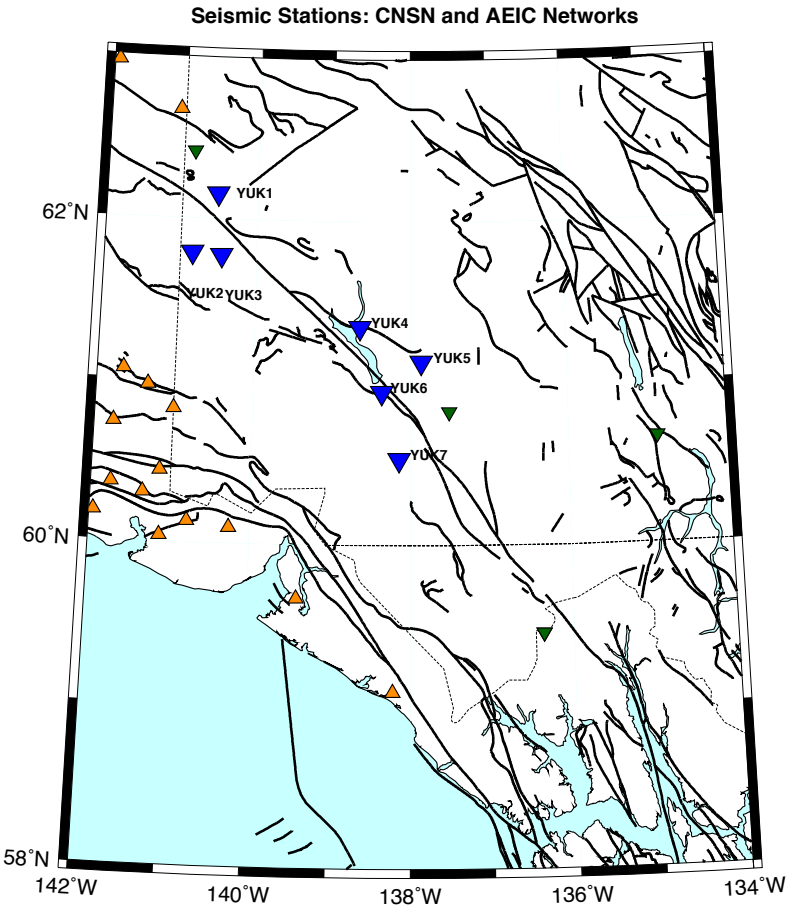


**Figure 10: Location of seismic stations of the CNSN and AEIC Networks used in this study. Inverted triangles are stations in the CNSN network; blue inverted triangles are YUK stations; green inverted triangles are the original stations of the CNSN network; orange triangles are seismic stations of the AEIC network.**

**Table 3: CNSN network of seismic stations, latitude and longitude and locations.**

| CNSN Network | Latitude | Longitude | Location |
|---|---|---|---|
| BVCY | 62.4141° | -140.8606° | Beaver Creek, YT |
| HYT | 60.8250° | -137.5038° | Haines Jct., YT |
| PLBC | 59.4567° | -136.3650° | Pleasant Camp, BC |
| WHY | 60.6597° | -134.8806° | Whitehorse, YT |
| DAWY | 64.0655° | -139.3909° | Dawson, YT |
| | | | |
| YUK1 | 62.1533° | -140.5287° | Sand Pete Hill, YT |
| YUK2 | 61.7868° | -140.8426° | White River, YT |
| YUK3 | 61.7755° | -140.4595° | Moose Creek, YT |
| YUK4 | 61.3448° | -138.6462° | Talbot Arm, YT |
| YUK5 | 61.1315° | -137.8593° | Granite Creek, YT |
| YUK6 | 60.9432° | -138.3626° | Outpost Mountain, YT |
| YUK7 | 60.5307° | -138.1399° | Dusty Glacier, YT |

**Table 4: AEIC network of seismic stations, latitude, longitude and locations. Stations in bold are part of the STEEP network.**

| AEIC Network | Latitude | Longitude | Location |
|---|---|---|---|
| CTG | 60.9657° | -141.3382° | Chitna Glacier |
| **GRNC** | 60.7319° | -141.7538° | Granite Creek |
| **LOGN** | 60.8245° | -141.0028° | Logan Glacier |
| PIN | 60.0967° | -140.2566° | Pinnacle |
| PNL | 59.6663° | -139.4017° | Peninsula |
| **SAMH** | 60.1298° | -140.7809° | Samovar Hills |
| **TABL** | 60.4403° | -141.1423° | Table Mountain |
| **BARN** | 61.0599° | -141.6601° | Barnard Glacier, AK, USA |

Eight stations of the AEIC network were used together with the stations of the CNSN network for the Duke River Fault and NE-trend, (Table 3 and 4). Within the Duke River Fault and NE-trend, there are 2215 P and S arrival picks (Figure 11).

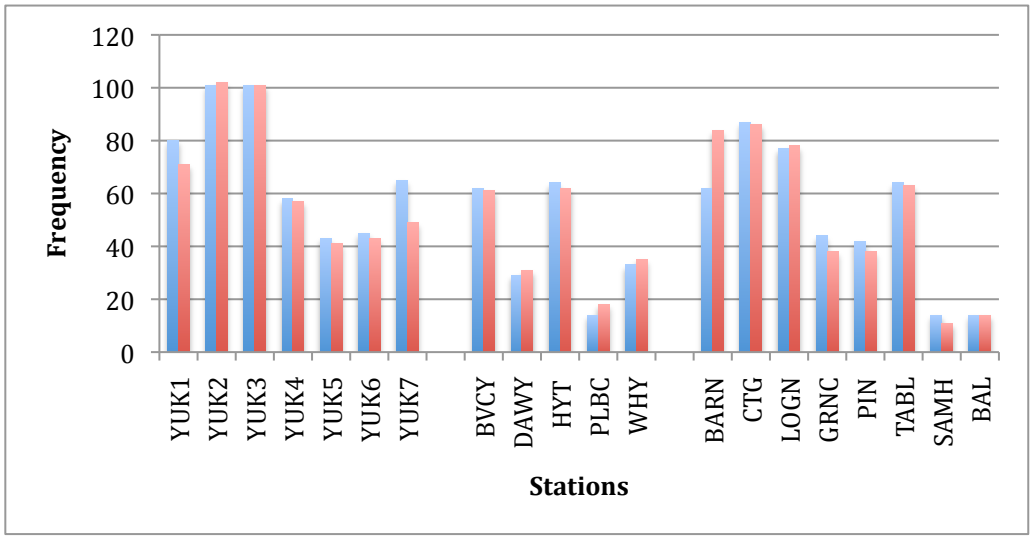


**Figure 11: Frequency of P (blue) and S (red) arrival picks the CNSN and AEIC network stations for the Duke River Fault and NE-trend.**

YUK2 and YUK3, followed by YUK1, were most frequently used in locating events in the Duke River Fault cluster and NE-trend. Of the Alaska stations, BARN, CTG, and LOGN were most frequently used, but marginally less frequently than YUK2 and YUK3 (Figure 11). Using the AEIC network, I had better station coverage and thus improved earthquake locations. On average, at least three stations from each network were used to locate events within the Duke River cluster and NE-trend. Events in the northern and southern Denali Fault clusters were located using only stations of the CNSN network.

# Chapter 4: Results and Analysis

## 4.1 Improved Earthquake Detection and Seismicity Patterns

A detailed scan of all waveforms of the seven YUK stations was performed between September and November 2010. Over the three-month period, 404 events were located (Figure 12). Magnitudes were between 0 and 3.0 and depths ranged from 0 and 30 km.

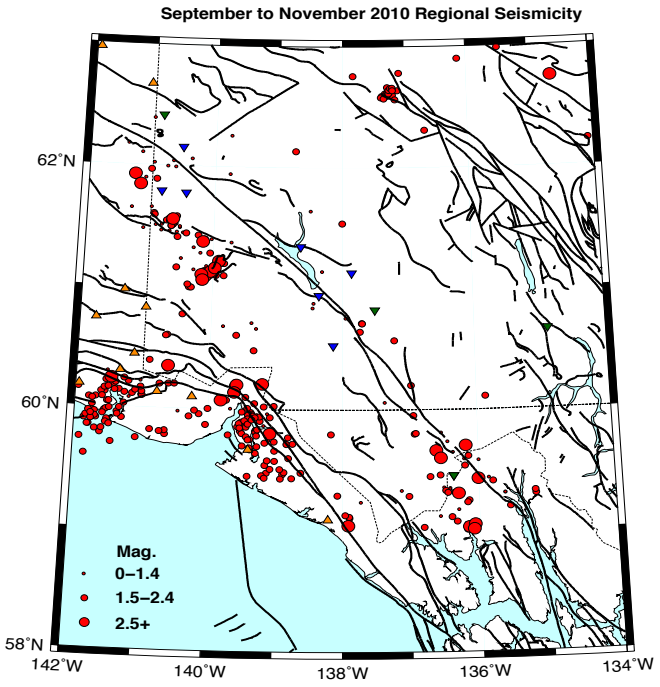


**Figure 12: Map of earthquakes (red circles) in southwest Yukon between September and November 2010. YUK stations are inverted blue triangles; other broadband CNSN stations used to locate earthquakes are inverted green triangles; orange triangles are Alaska stations.**

The increased capability to detect earthquakes in the region is clearly illustrated by considering three-month (September-November) plots of seismicity from 1985 to present in 5-year increments. Figures 13a and 13b show pre-YUK array seismicity patterns for 1985 and 2005. (see Appendix C for seismicity plots for the same time window for 1990, 1995 and 2000) In contrast Figure 13c shows earthquakes immediately after installation of the YUK array (September-November 2010). The addition of a new cluster of seismicity, the NE-trend, is clearly illustrated. There are also many more events detected along the Duke River Fault. An additional 268 events were located between September and November 2010, with magnitudes ranging between 0.02 and 2.44 and depths between 0 and 30 km.

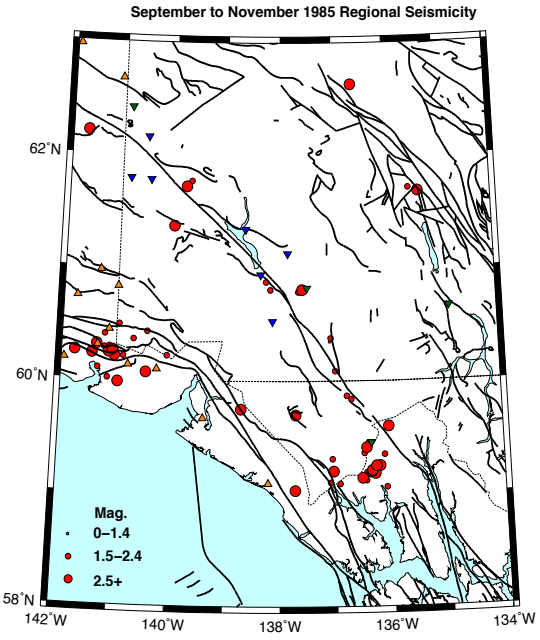


**Figure 13a: Regional seismicity, September to November 1985.**

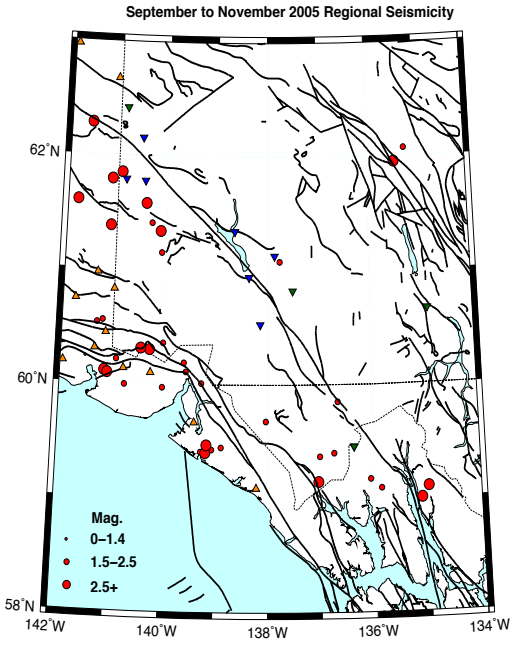


**Figure 13b: Regional seismicity, September to November 2005.**

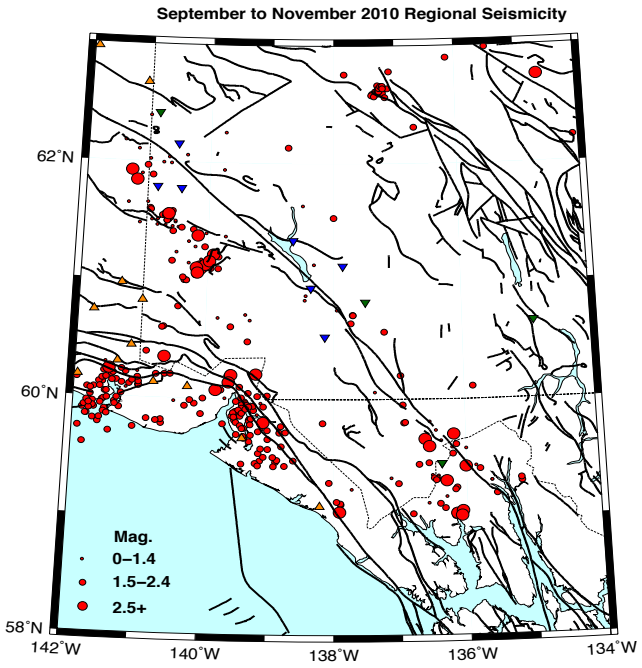


**Figure 13c: Regional seismicity, September to November 2010.**

Figure 14 illustrates regional seismicity over a 15 month period following installation of the YUK array. 980 events were located during this period with magnitudes between 0.2 and 4.7 and focal depths between 0 and 35 km. Seismicity can be divided into four main areas: 1) Yaktutat Block-Fairweather fault, 2) Duke River Fault, 3) Denali Fault, and 4) NE-trend. There is relatively little seismic activity during this period along the northern Denali Fault and only a small amount of activity along the southern portion of the Denali Fault. There is significantly more seismic activity along the Duke River Fault and NE-trend, and much seismicity just west and parallel to the Alaska-Yukon border between the Duke River Fault and northern Denali Fault (Figure 14). Figure 15 illustrates the four clusters of earthquakes I focus on during the 15 month period.

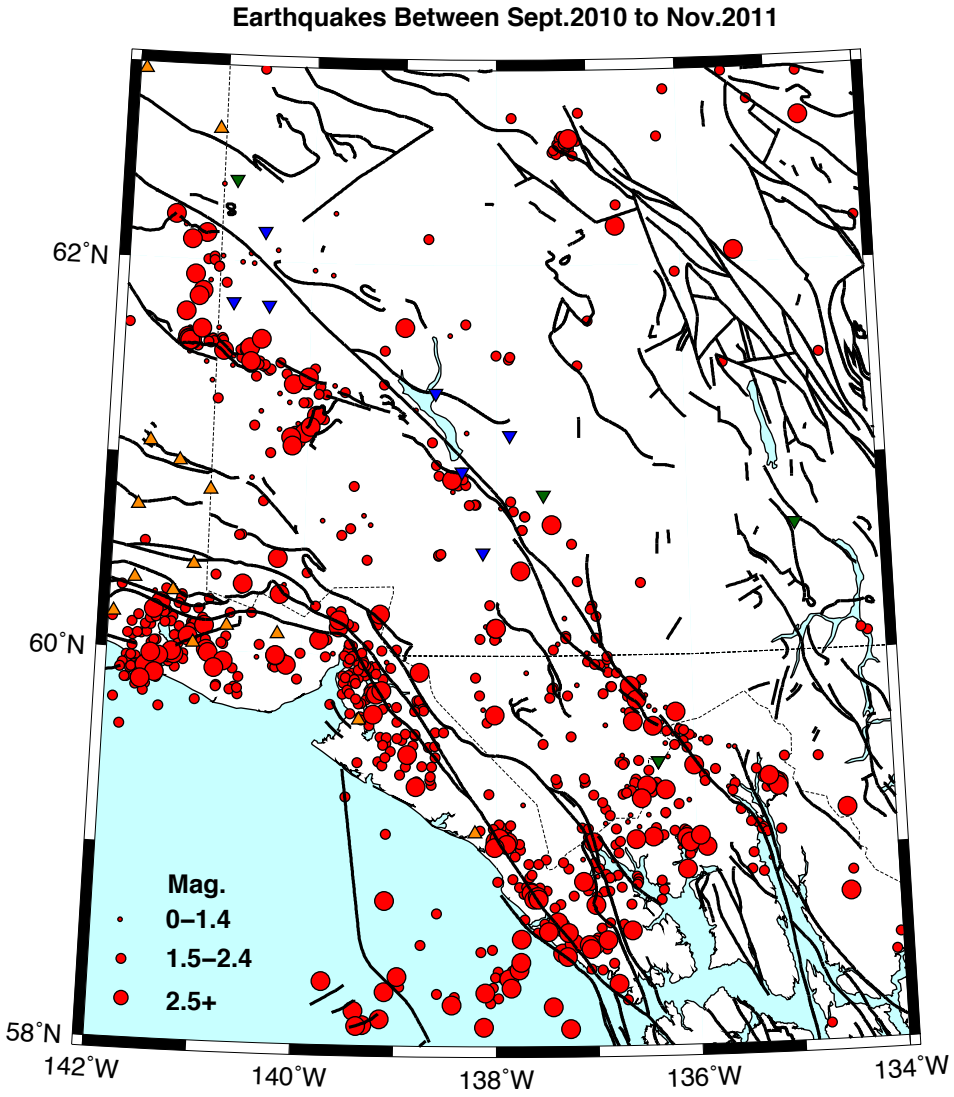


**Figure 14: Regional seismicity between September 2010 and November 2011.**

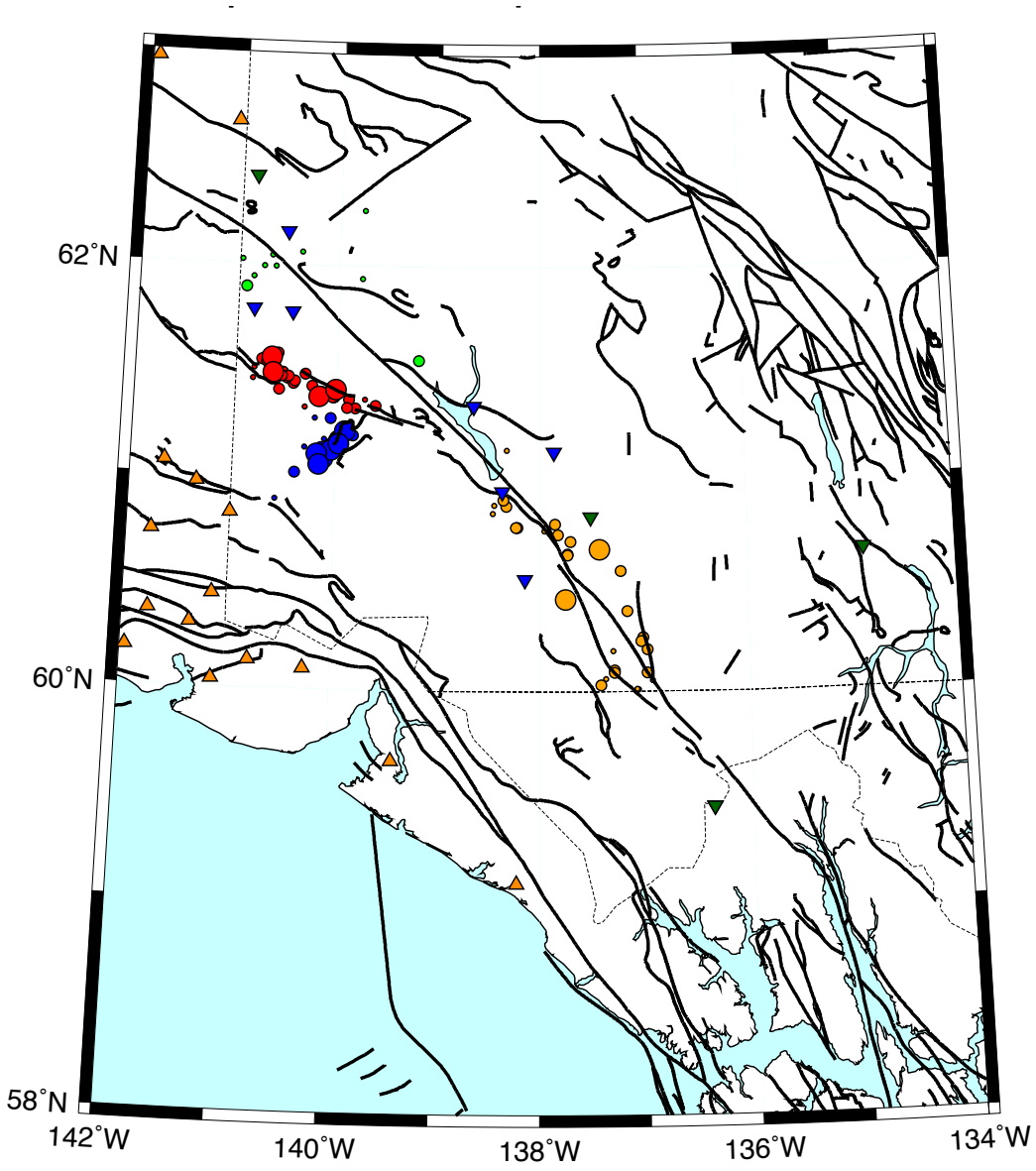


**Figure 15: Location of earthquakes within each of the four clusters between September 2010 and November 2011. Blue circles are events in the NE-trend; red circles are events in the Duke River Fault cluster; lime green circles are events in the northern Denali Fault segment; and yellow circles are events in the southern Denali Fault segment.**

## 4.2 Improvement in Single Event Locations Using the YUK Array

To quantify how the new YUK array has improved earthquake locations and depths in southwest Yukon, events that were located in the Duke River cluster and NE-trend were located using only the original CNSN network (not including the YUK array) and compared to the locations of these events including the YUK array. In the two clusters, 37 of 106 events can be located using only the original CNSN network. Only 13 of these 37 events had reliable locations. Depths were kept consistent when relocating these 13 events to reduce changes in locations due to differences in depth. The shift in location of events can be viewed as a mislocation prior to the YUK array. There is an average mislocation of about 6.9 km and a general shift to the southwest after including the YUK array (Figure 16). However, there are not enough events to reliably conclude that the shift in all event locations will be to the southwest. The shift of locations southwest may be biased because all stations are located north and east of the NE-trend. Thus, the location of the stations give good control in the northeast direction, however poor control in the southwest direction. S-wave arrival times are more difficult to pick because it arrives in the coda of the P-wave which results in a larger signal-to-noise ratio (Husen & Hardebeck, 2010). This often results in a delayed pick of the S-wave arrival and consequently measures a farther distance from each station. This may explain the general shift southwest of the locations in the NE-trend after including the YUK array. (Havskov & Ottemoller, 2010)

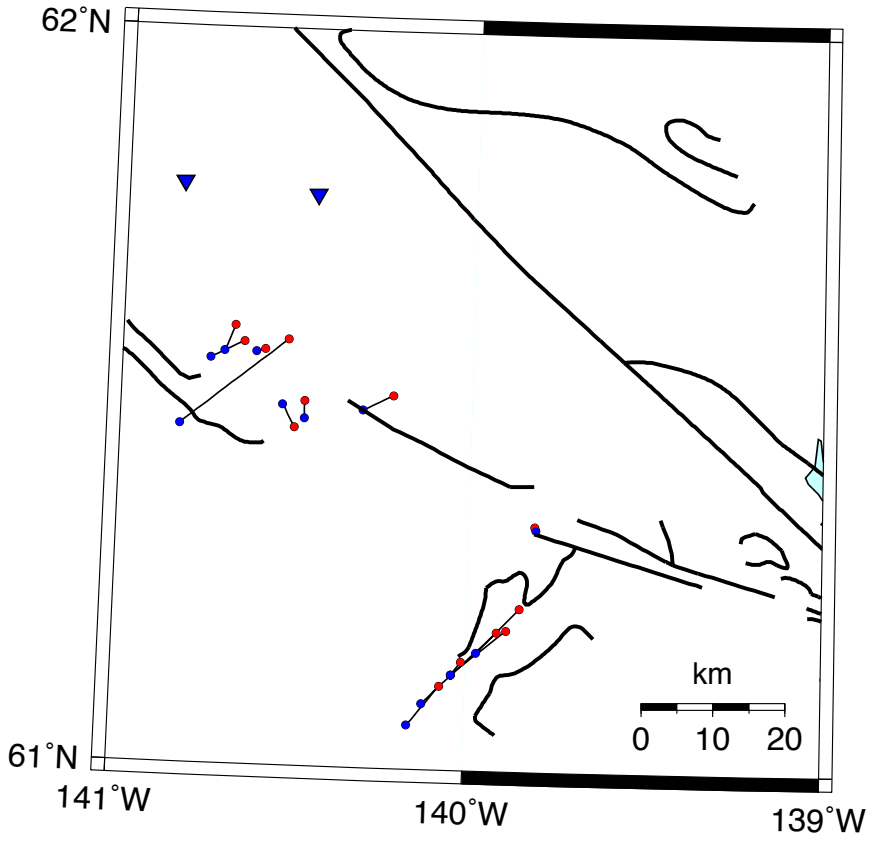


**Figure 16: Mislocation of events from the original CNSN network to an array that includes the YUK array in the NE-trend and Duke River Fault. Red circles are original network locations and blue circles are locations that include the YUK array.**

Comparing the uncertainty in locations of these events (Figure 16), the maximum horizontal error reduces from ±6.8 km without the YUK array to ±2.0 km with the YUK array.

With the addition of the YUK array, the aftershock sequence of the M4.3 earthquake on 3 August, 2011, just west of the Alaska-Yukon border near the Denali Fault was detected (Figure 17). Only one foreshock was recorded prior to the mainshock and nine aftershocks occurred during the week following the mainshock. Aftershocks ranged in magnitudes from 1.4 and 0.7. Each of the aftershocks was located consistently using the

same four stations (BVCY, YUK1, YUK2, and YUK3) and a fixed depth at 10 km (average depth of earthquakes in the southwest Yukon).

To quantify the effects of the YUK array on the location of the 3 August 2011 earthquake, the mainshock was located with and without the YUK array. There was less than a 1 km shift in the location of the mainshock. Free depths were 7.4 km with the YUK array and 10.2 km without the YUK array. However, the closest station (YUK1) is about 40 km from the mainshock and so depths are not well-constrained. The depth of the mainshock is not well-constrained because the distance to the closest station is greater than the depth of the earthquake.

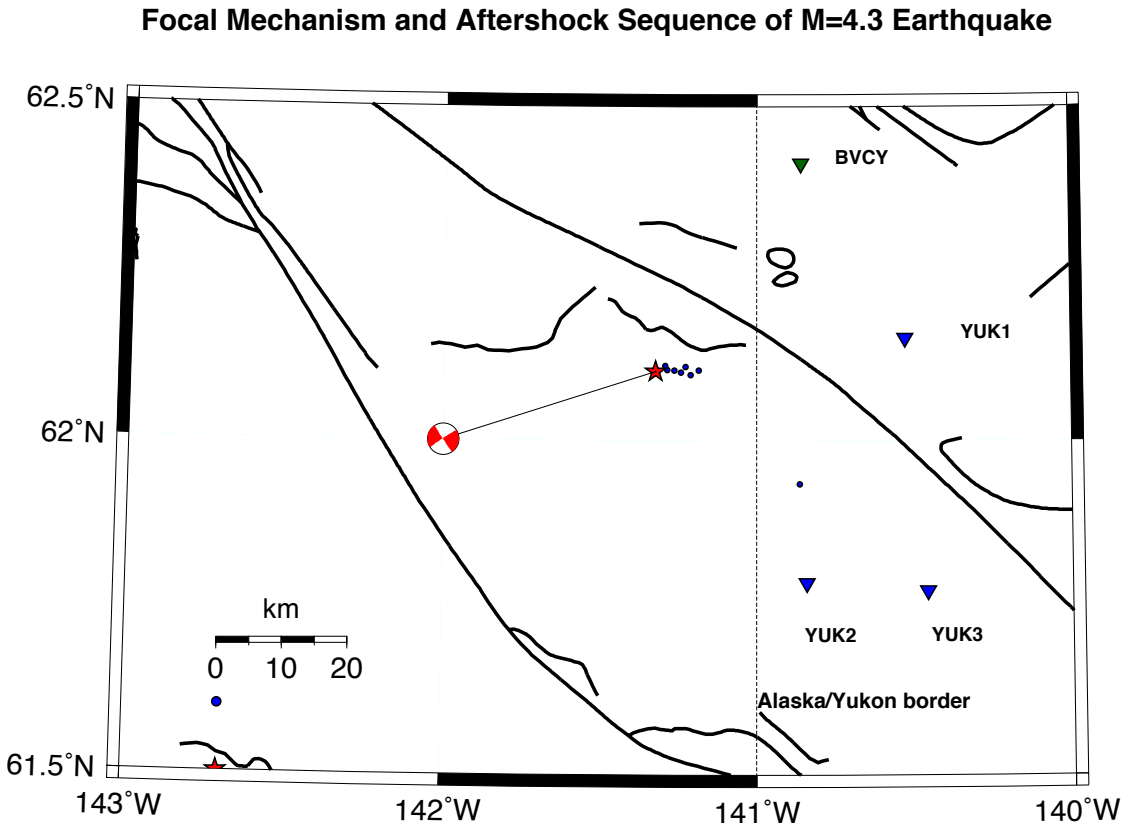


**Figure 17: Mainshock, aftershock sequence and focal mechanism for events following the 3 August 2011 mainshock.**

The focal mechanism for the M4.3 mainshock was computed using CMT inversion (Kao et al., 2011). It shows predominately strike-slip motion along either a mainly ENE-trending fault or WNW fault. Aftershocks align E-W in this case.

### 4.3 Identification of Active Structures using Progressive Multiple Event Location

The Progressive Multiple Event Location (PMEL) program (Pavlis, 1983) better identifies and constrains spatial patterns of earthquakes by reducing uncertainties in locations and depths. This, in turn, enables for better identification of active structures in a region. I am particularly interested in determining the source of the seismicity from within the Duke River cluster and NE-trend and their source of seismicity.

PMEL was first performed using only the CNSN network for the Duke River cluster and NE-trend between September 2010 and November 2011. Initially I set up a grid that included events of the CNSN network within the Duke River Fault, NE-trend, and extending to the mainshock-aftershock sequence on the northern Denali Fault near the Alaska-Yukon border. Each grid point is separated by a horizontal distance of 25 km and a vertical distance at a depth of 5 km. Each cluster has a minimum of 10 events. These events are selected within a minimum radius of 17.7 km and a maximum radius of 25 km; and depth range of 10 km. There is a minimum radius of 17.7 km and a maximum radius of 25 km. The minimum radius is calculated from the maximum radius divided by the square root of 2 to ensure outliers are not included. There are a total of 209 single events within the grid. Of the 209 events, 70 events have free depths; after performing *dbpmel* the total number of locations was reduced to 179. Such a reduction was expected as

events are excluded in *dbpmel* if the rms location error is significantly larger than those of the other events within the cluster.

To improve station geometry, the AEIC network was then merged with the CNSN network, 106 single event locations within the two clusters; 82 of the 106 events have free depths. Some events within the two clusters of the CNSN network were not included because they did not have arrival time picks from any of the AEIC stations. *dbpmel* was performed on the new single event locations of the combined networks, yielding 93 *pmelavg* locations. Figure 18a-d illustrates the transition from the original single event locations using the CNSN network to single event locations using the combined networks and each of their corresponding *pmelavg* locations.

Cross-correlation using *dbxcor* was attempted at stations YUK2 and YUK3. Seismic waveforms of each event defined by each cluster were stacked iteratively for the two stations. However, the waveforms of each event had too much variation to perform cross correlation. *dbxcor* could still be very used to reduce errors in the arrival time picks by comparing P arrivals within each stack of waveforms for a cluster of events, but was not done in this study.

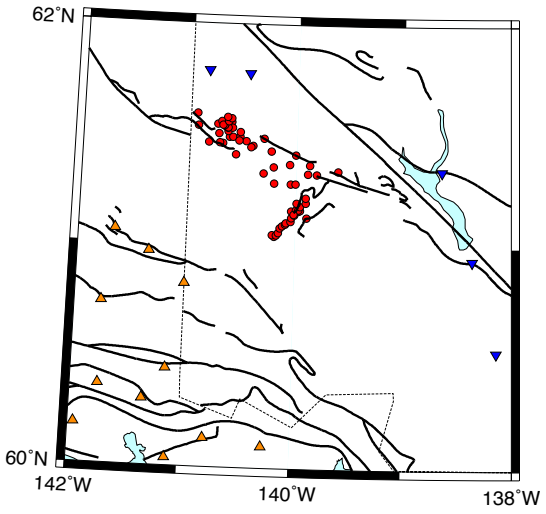


**Figure 18a: Single event locations using the CNSN network. Total number of events =124.**

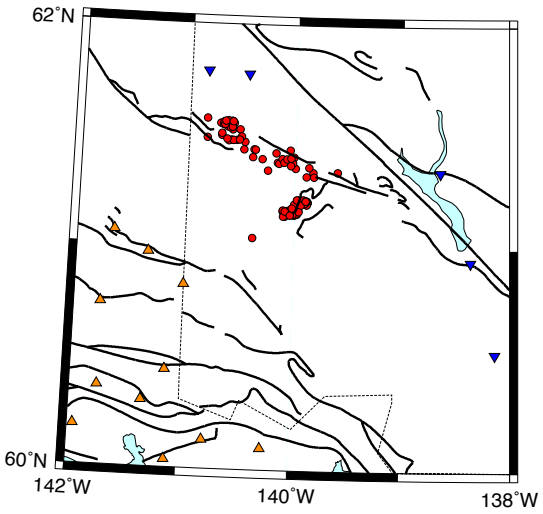


**Figure 18b: Single event locations CNSN and AEIC networks. Total number of events = 106.**

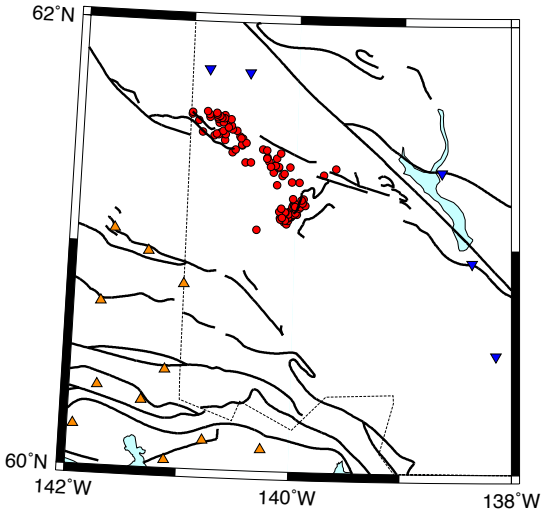


**Figure 18c: *dbpmel* locations using the CNSN network. Total number of events = 116.**

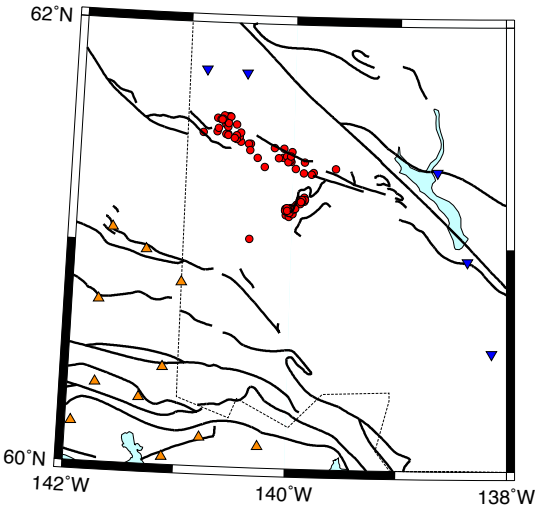


**Figure 18d: *dbpmel* locations using combined CNSN and AEIC networks. Total number of events = 93.**

The NE-trend tightens to the northeast when single event locations of the CNSN network (Figure 18a) are compared to single event locations of the combined CNSN and

AEIC networks (Figure 18b). For the events in the NE-trend there is an average mislocation of ~6.6 km (Figure 19) to the northeast and an average decrease in depth of 2.6 km. Single event locations within the Duke River cluster and NE-trend for the CNSN network (Figure 18a) have an average maximum horizontal error of ±2.3 km and average error in depth of ±2.1 km. For the combined CNSN and AEIC networks (Figure 18b), single event locations have an average maximum horizontal error of ±0.9 km and an average error in depth of ±3.2 km.

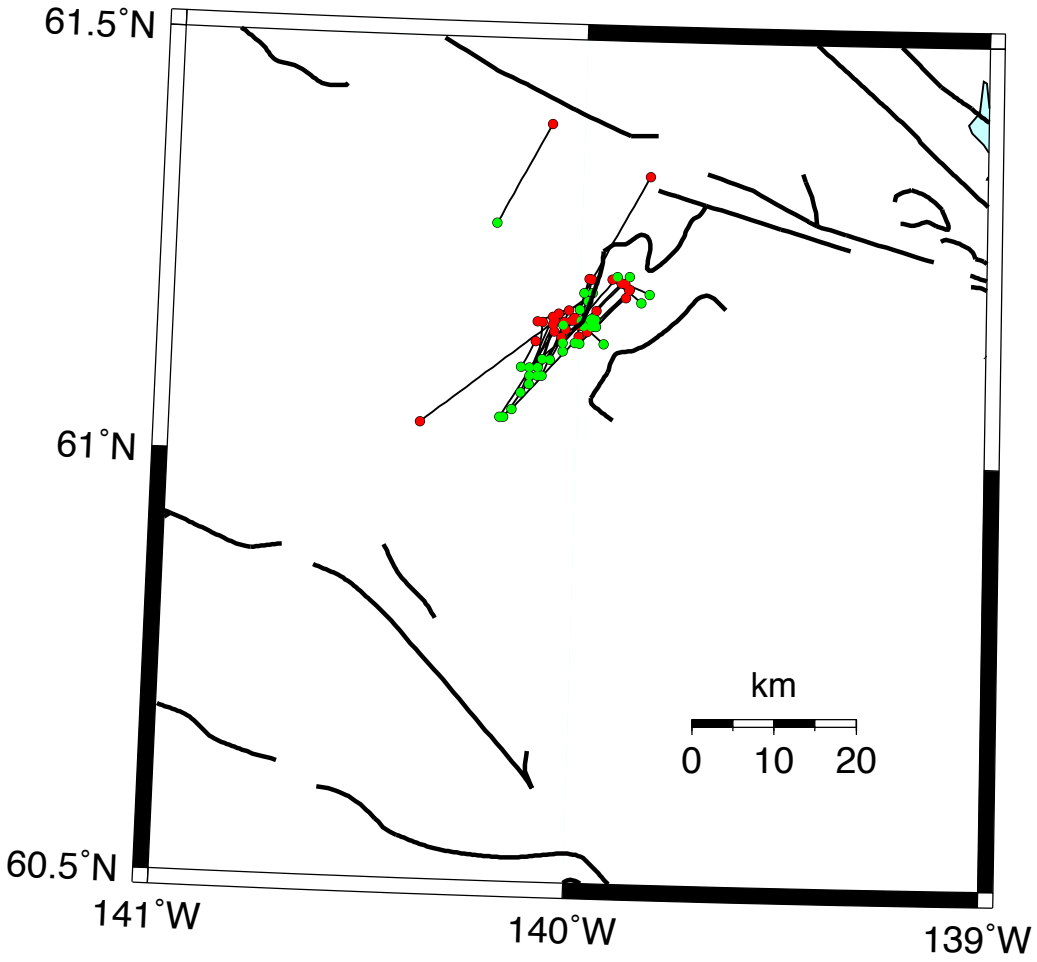


**Figure 19: Shift of single event locations of the CNSN network (green) to single event locations of combined CNSN and AEIC networks (red).**

With an improved station geometry, NE-trend locations shift noticeably northeast. This shift of locations is most likely a result of more precise locations due to a better station geometry. Another possibility explanation for the shift northeast may suggest the velocity model for this region is not the most suitable.

When *dbpmel* was performed with the combined network (Figure 18d) two distinct linear trends became apparent along the Duke River Fault, and the total length of NE-trend decreased along a northeast-trending fault branching off the Duke River Fault. As expected, identification of active structures is most clearly defined when performing *dbpmel* on single event locations of the combined network (Figure 18d). For events within the NE-trend, there is an average shift of 1.8 km to the southwest from the single event locations to the *dbpmel* locations of the combined network and within uncertainties there is no change in depth. The mislocation describes the shift in event locations from after running *dbpmel* and after adding in the Alaska Regional Network. The NE-trend decreased in length from 30.6 km to 12.3 km.

There is significant reduction in location uncertainties from single event to *pmelavg* locations. For the combined network, there is an average rms error of ±0.4 s for the single event locations compared to an average global rms error for the *pmelavg* locations of ±0.07 s.

Change in latitude and longitude between single event locations and *pmelavg* locations for the Duke River cluster and NE-trend are illustrated in Figures 20 and 21. After performing *dbpmel* on the single event locations there is a modal change in latitude of 0.02° north, with two large changes in longitude at -0.01° and +0.03° west. The bi-modal

distribution in longitude may be due to the Duke River Fault and NE-trend having different longitudinal shifts.

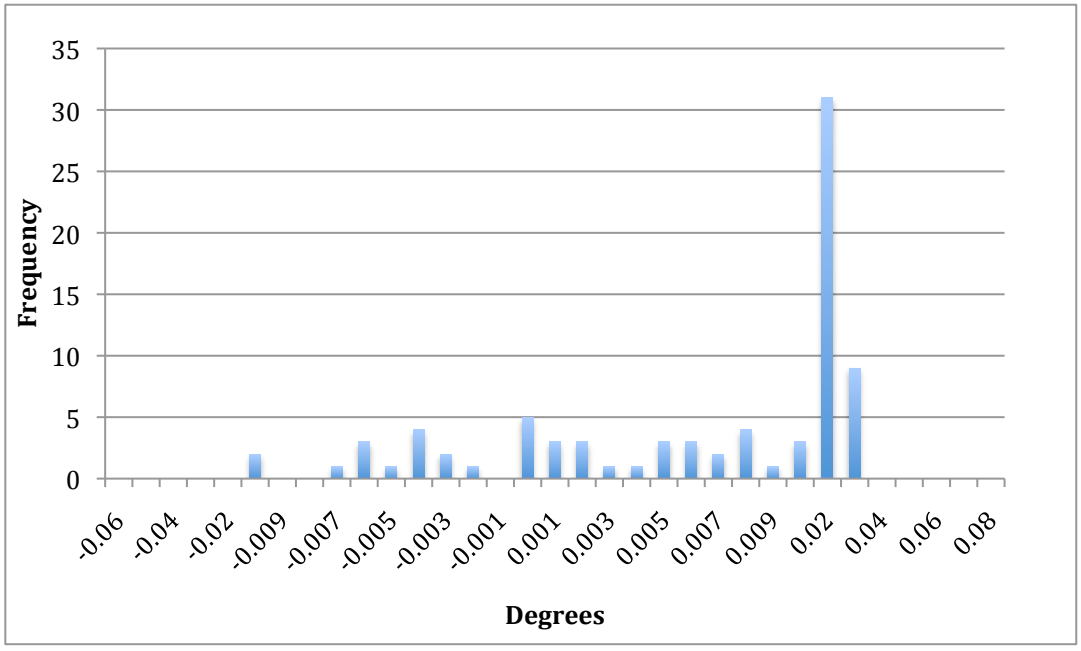


**Figure 20: Latitude difference between single event and *pmelavg* locations for the combined network for the Duke River cluster and NE-trend.**

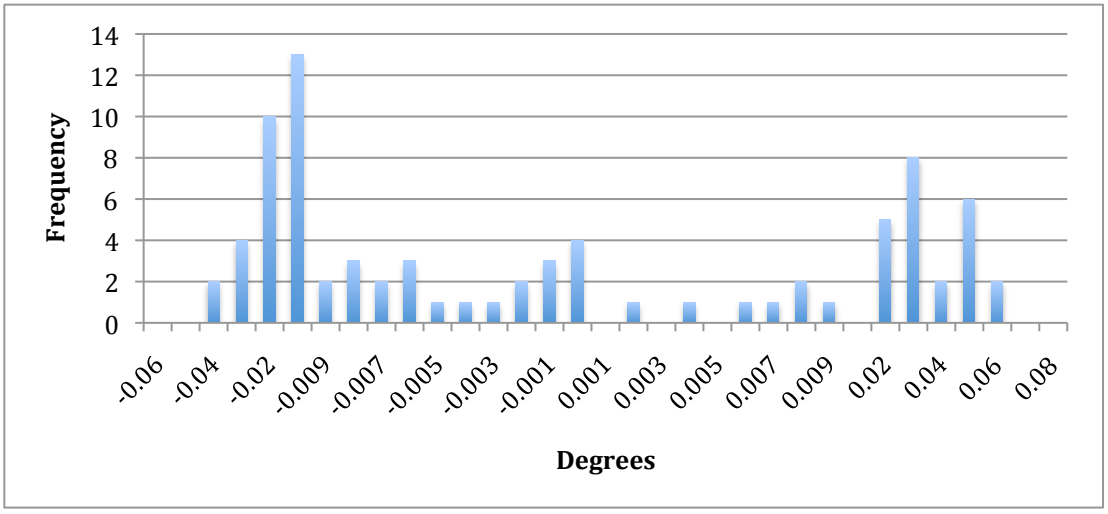


**Figure 21: Longitude difference between single event and *pmelavg* locations for the combined network for the Duke River cluster and NE-trend.**

## 4.4 Depth Analysis

One of the most important outcomes of the addition of the new YUK array and the AEIC network is the ability to compute focal depths more accurately. The increase in the number of stations and improved station geometry allows for better constraints on depths (free depths) compared to the prior CNSN catalogue where very few depths could be calculated. The overall free depth range for the southwest Yukon based on 179 events between September 2010 and November 2011 (Figures 22 and 23) of the CNSN network is 0-30 km, with an average depth of 10.9 km.

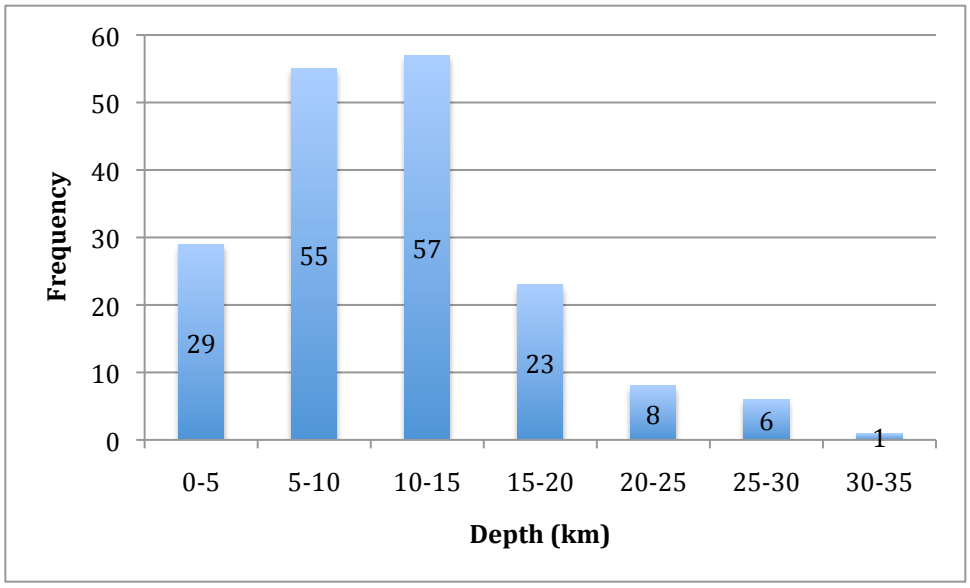


**Figure 22: Histogram of 179 free depths in southwest Yukon between September 2010 and November 2011.**

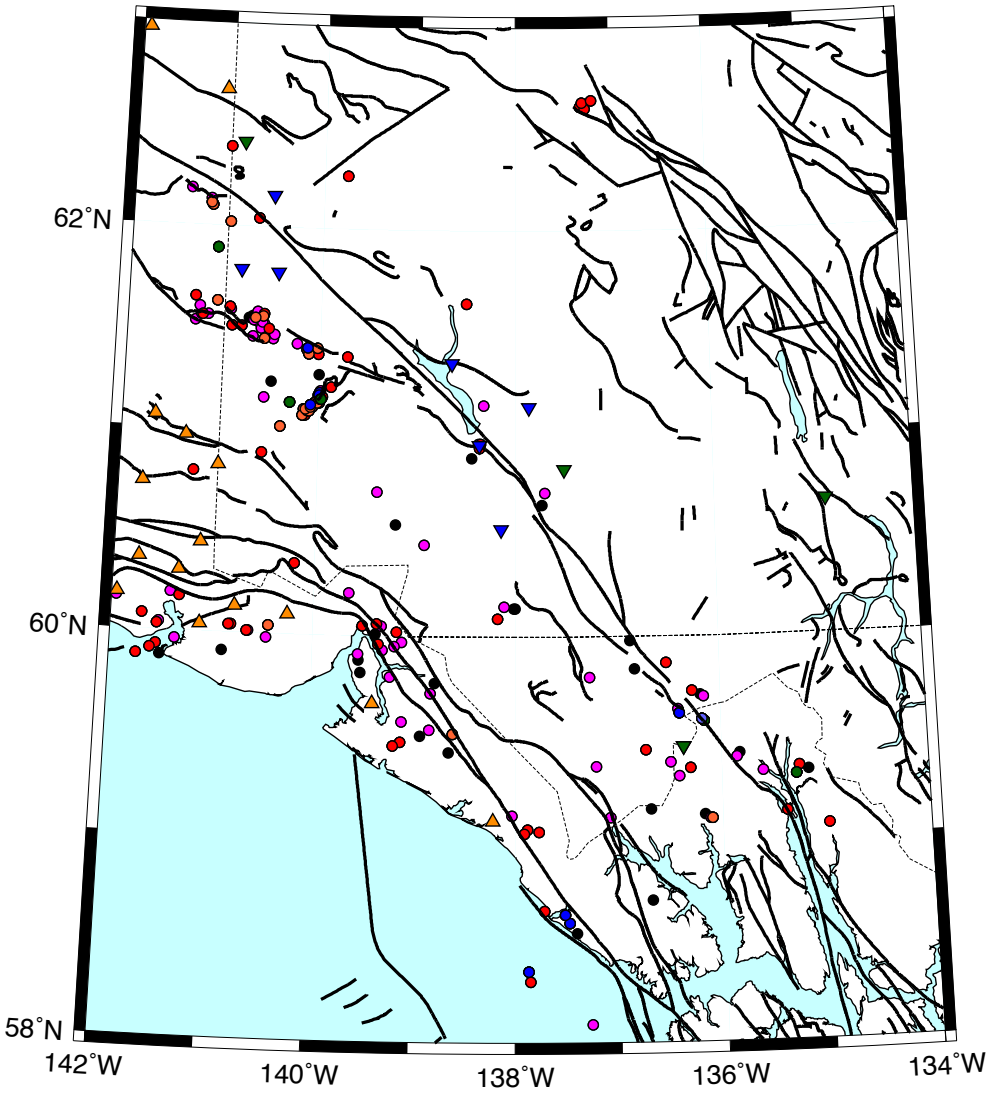


**Figure 23: Free depths of earthquakes in southwest Yukon between September 2010 and November 2011, corresponding to histogram in Figure 21. Black circles are depths from 0-5 km; magenta circles are depths of 5.1-10 km; red circles are depths of 10.1 -15 km; orange circles are depths of 15.1-20 km; blue circles are depths of 20.1-25 km; green circles are depths of 25.1-30 km; and light blue represent depths between 30.1-35 km.**

Free depths of the Duke River Fault and NE-trend determined with the CNSN and AEIC networks are shown in Figure 24 and the corresponding histogram is shown in Figure 25. There were only 20 events prior to the YUK array that had free depths,

whereas 82 events with free depths were detected in the period from September 2010 to November 2011 after the YUK array was deployed. Between September 2010 and November 2011, depths range mainly between 0 and 20 km with an average of 10.6 ± 3.2 km. The NE-trend free depths are dominantly between 5-10 km and 15-20 km, with an average depth of 11.6 km. The Duke River Fault has free depths ranging from 0 to 20 km, with an average depth of 9.5 km. There does not appear to be any spatial trend of free depths on the Duke River Fault or within the NE-trend.

The Duke River events have better constrained depths than the NE-trend events. Earthquakes in the northern portion of the Duke River Fault are ~20-25 km from stations YUK2 and YUK3. Most of the events within the Duke River cluster, however, are less than 20 km deep and thus are not well constrained. Closest stations to the NE-trend are LOGN and YUK3 at a distance of 55-80 km. Events in the NE-trend are also typically less than 20 km deep and therefore depths are not well constrained.

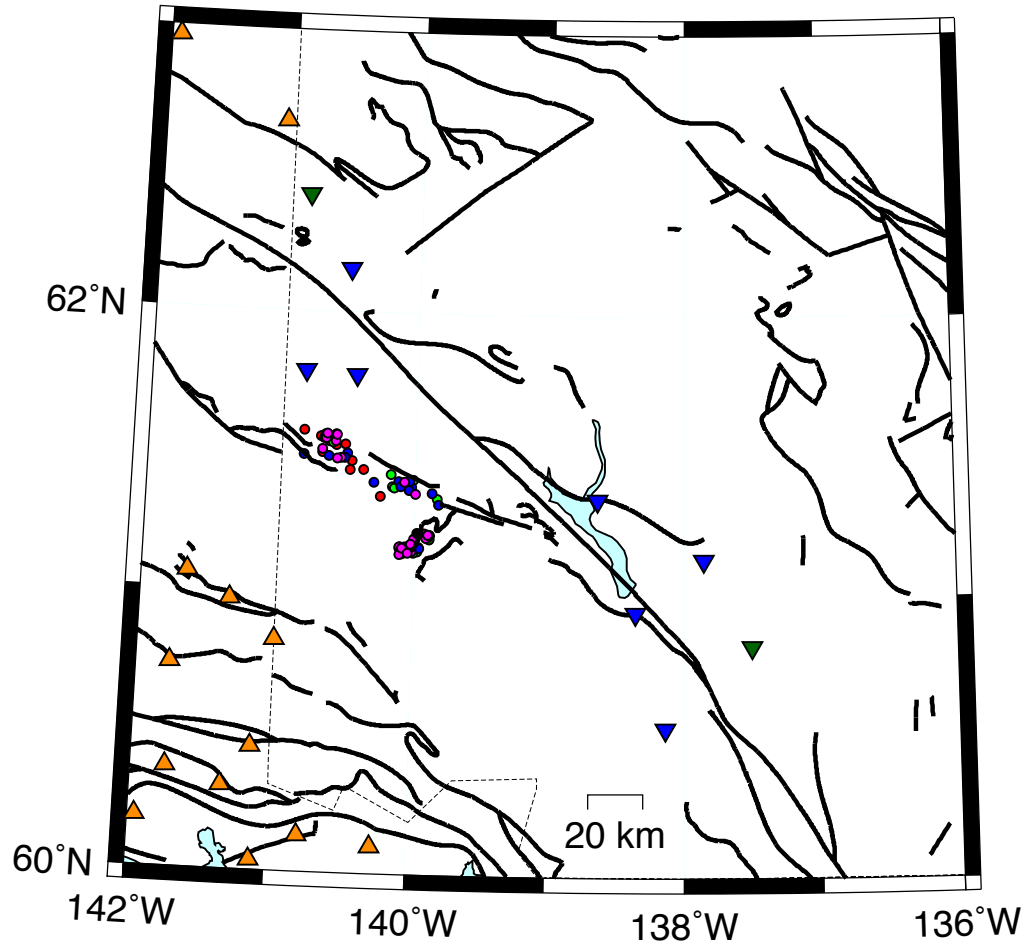


**Figure 24: Single event location free depths of the CNSN and AEIC networks for the Duke River Fault and NE-trend between September 2010 and November 2011. Red circles are depths from 0-5 km; green circles are depths of 5.1-10 km; blue circles are depths of 10.1-15 km; magenta circles are depths of 15.1-20 km; black circles are depths of 20.1-25 km; and light blue; are depths of 25.1-30 km.**

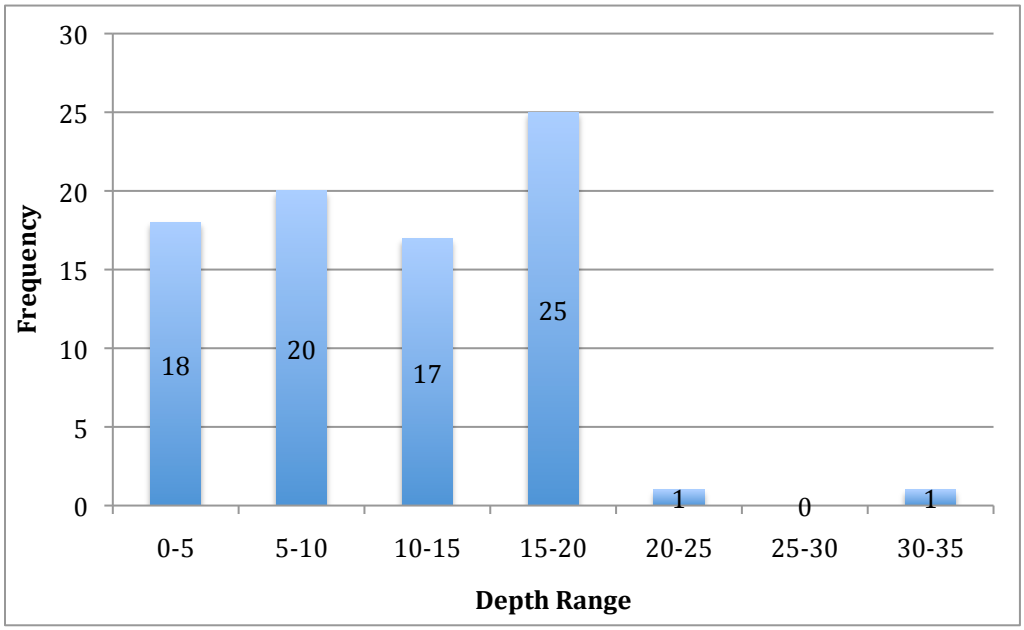


**Figure 25: Histogram of free depths for the Duke River and NE-trend clusters from September 2010 and November 2011. The number of free depths is 82.**

Two events in the southern Denali Fault segment that are only 5 km and 8 km from seismic station YUK6. The waveforms show an S-P time of 1.9 s (Figure 26a) and 2.2 s (Figure 26b). The waveforms are consistent with an upper crustal (2-10 km) focal depths.

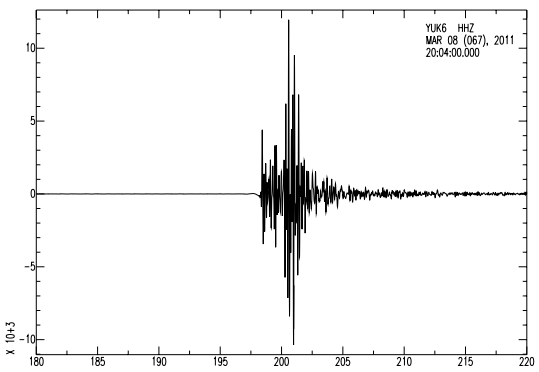


**Figure 26a: 8 March, 2011 HHZ. Vertical channel shows a distinct P-arrival, followed by an S-arrival by 1.9 s.**

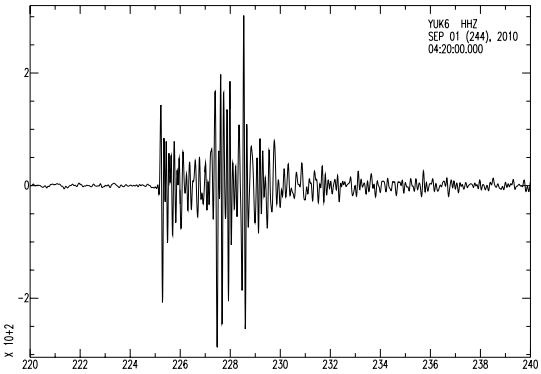


**Figure 26b: 1 September, 2010 HHZ. Vertical channel shows a distinct P-arrival followed by S-arrival by 2.2 s.**

## 4.5 Source of Earthquakes in the NE-Trend

I explore several different possibilities for the source of the earthquakes in the NE-trend: 1) tectonic; 2) glacier or ice related; 3) variations in water pore pressures; and 4) surface loading or modifications to the stress regime. A Google Earth image (Figure 27) shows that the NE-trend events, which are located between Kluane Glacier and Steele Glacier, lie along a northeast trending fault line south of the Duke River Fault.

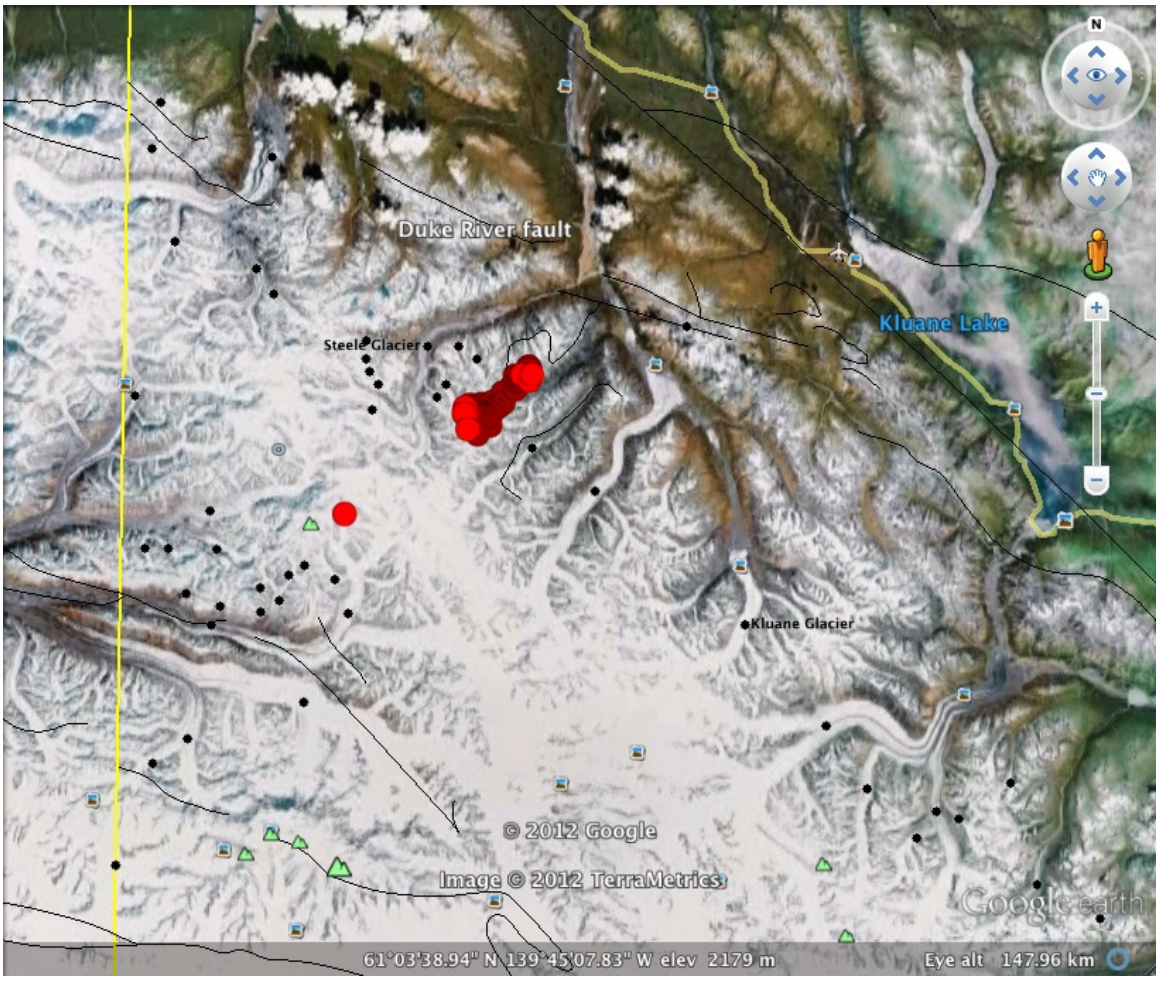


**Figure 27: Google Earth map view of the NE-trend *pmelavg* locations between Steele Glacier and Kluane Glacier. Black dots are different glaciers. Green triangles are different mountains.**

To address whether these earthquakes are tectonic, I compared the seismic characteristics of the Duke River Fault events, which are confirmed tectonic earthquakes, with the NE-trend events. Using CNSN catalogue and SAC software, I analyzed seismic characteristics of five random events within both the Duke River Fault and NE-trend, all occurring during September and October of 2010 and recorded at station YUK3.

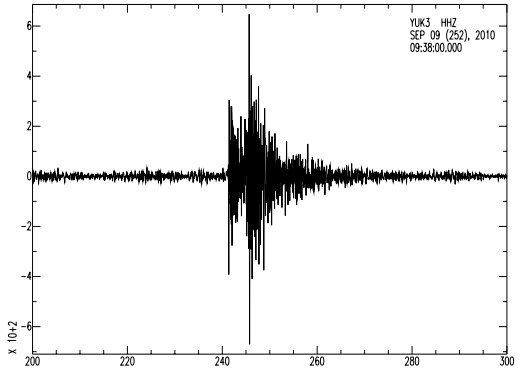


**Figure 28a: YUK3 HHZ of Duke River event 9 September, 2010.**

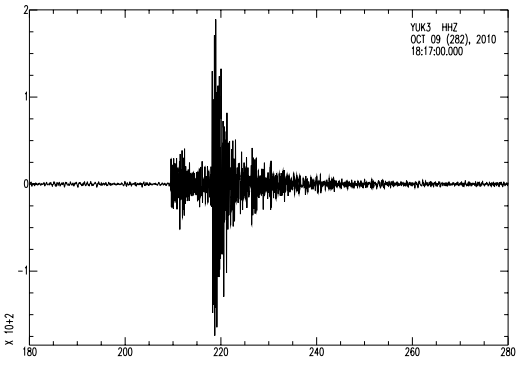


**Figure 28b:YUK3 HHZ of NE-trend 9 October, 2010.**

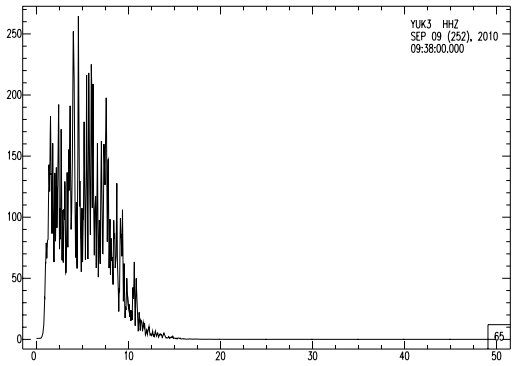


**Figure 28c: Frequency spectrum of Duke River event, 9 September, 2010.**

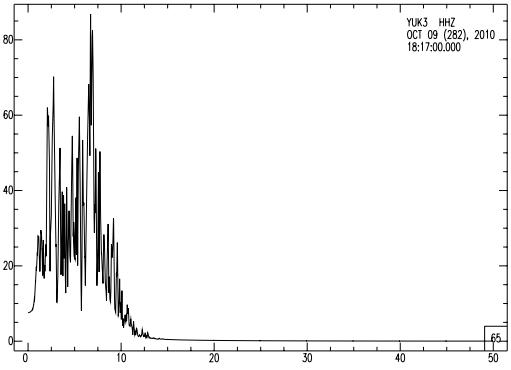


**Figure 28d: Frequency spectrum of NE trend event 9 October, 2010.**

The waveforms of the NE-trend event (Figure 28b and 28d) have very impulsive P and S arrivals and typically show peaks at ~2.5 Hz and ~7.5 Hz (Figure 28d). The Duke River Fault event (Figure 28a and 28c) has generally impulsive P arrivals but more emergent S arrivals and dominant frequencies of ~5 Hz (Figure 28c). The seismic characteristics are similar enough that these events are probably tectonic in origin. The depths of the two clusters have a similar range of 0-20 km and both have an average depth of about 10 km.

After relocating the NE-trend events using *dbpmel*, I found that the events align with a map surface fault (R. Kung, personal communication) (Figure 27), further suggesting that these events are tectonic. The *b*-values of the NE-trend are relatively high (b≈ 1) but typical of *b*-values of tectonic events based on the frequency-magnitude statistics between 1985 and 2011.

Next I considered whether the NE-trend events could be glacier or ice related. I looked at two aspects: 1) seasonality and 2) seismic characteristics. The NE-trend events appear to be seasonal, with 68 of 75 events occurring between September and November 2011. To address whether these events are seasonal, smaller events having an S-P time of ~10 s at YUK3, consistent with the NE-trend, were located for each month during 2011. About one event was detected each month, except between August and October (Figure 29).

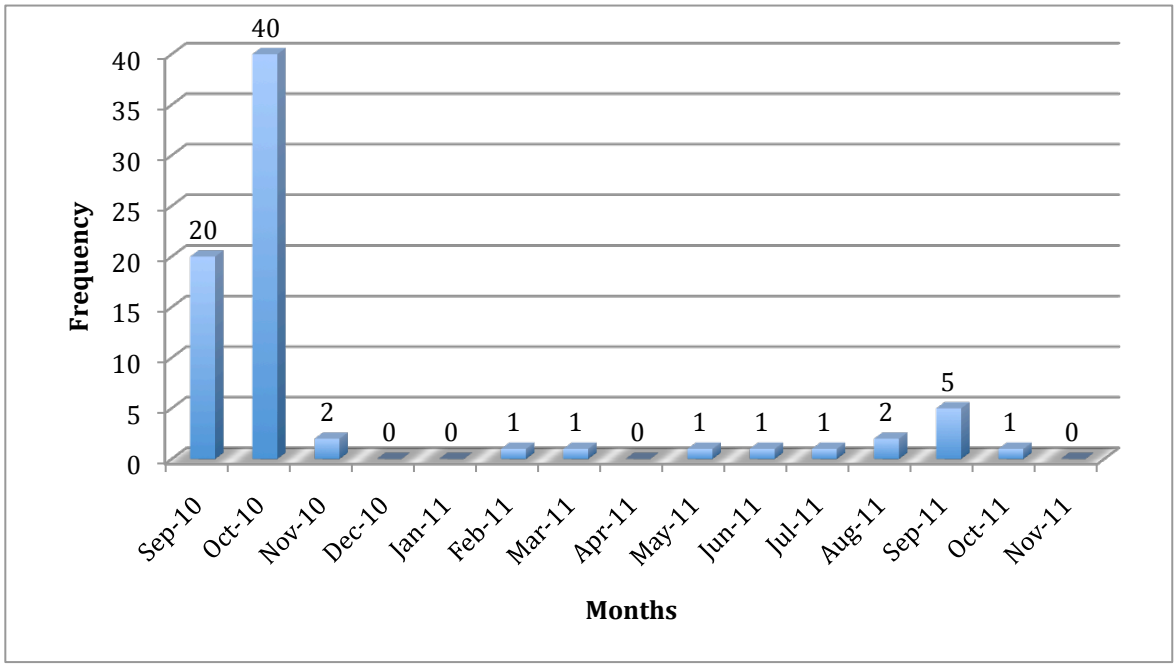


**Figure 29: Frequency of events each month within the NE-trending cluster between September 2010 and November 2011. Total of 75 events.**

Prior to the YUK array, events were first detected within the NE-trend in 1992 and randomly occurred throughout the following years. There were 32 events between January 1992 and September 2010, with no indication of seasonality.

I used the seismic characteristics to determine if the NE-trend events were common before the YUK array. Prior to the installation of the YUK array, the seismic station HYT (close to Haines Junction) was the nearest station to the NE-trend. I chose selected YUK array events, and paired them with events of the same magnitude that occurred prior to the establishment of the YUK array. The S-P time is about 15-17 s and both waveforms have emergent P and S arrivals times. The vertical channels of the waveforms are similar (Figure 30a and 30b).

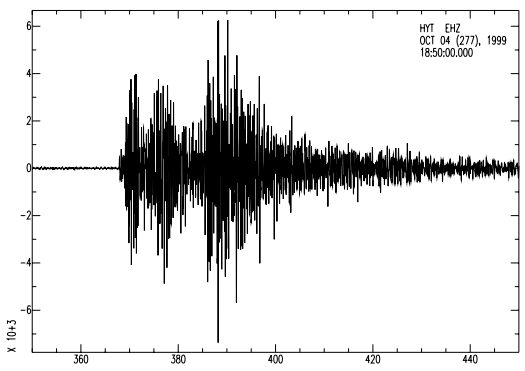


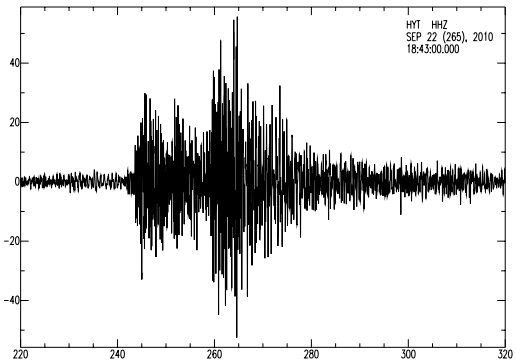


**Figure 30a: HYT EHZ, 4 October, 1999.** **Figure 30b: HYT HHZ, 22 September, 2010.**

Additionally, there may have been many small events (M<2.0) not located prior to the YUK array due to the sparse network. I selected a random year prior to 2010 to search the CNSN database for local events that were listed as "too small" to be located at station HYT and so had not been located as part of the catalogue. There were 46 of these events in 2000 and 130 events in 2005. However, many of these events do not necessarily originate from the NE-trend. In 2000, a random selection of 16 of the 46 events (about two events per month), yielded 5 events that have an S-P time of 15-17 s and so may have originated in the NE-trend. In 2005, a random selection of 24 events (two per month) yielded only 1 event with an S-P time of 15-17 s.

There is not very conclusive evidence prior to the YUK array that NE-trend events are seasonal. Several years more data will be required to draw reliable conclusions as to whether the NE-trend events predominately occur between September and November.

Next I examine two types of ice or glacier-related seismicity. 1) "icequakes" - seismic events with high frequency and short duration that are caused by cracking or fracturing within glaciers. Icequakes are similar to small, shallow tectonic earthquakes, with energy releases that is typically less than 1 J. Since the NE-trend events have depths between 0

and 20 km and energies between $10^4$ to $10^7$ J, they are too large and too deep to be icequakes.

2) "Glacierquakes" - seismic events of longer duration and low frequency caused by basal slip or large calving events. These events are detected at distances exceeding 200 km on the regional network (Wolf et al., 1997). Glacierquakes are emergent, monochromatic, non-dispersive waveforms that have dominant frequencies of 1-2 Hz (Figure 31a and b). The NE-trend events have very impulsive waveforms with a greater range of composite frequencies.

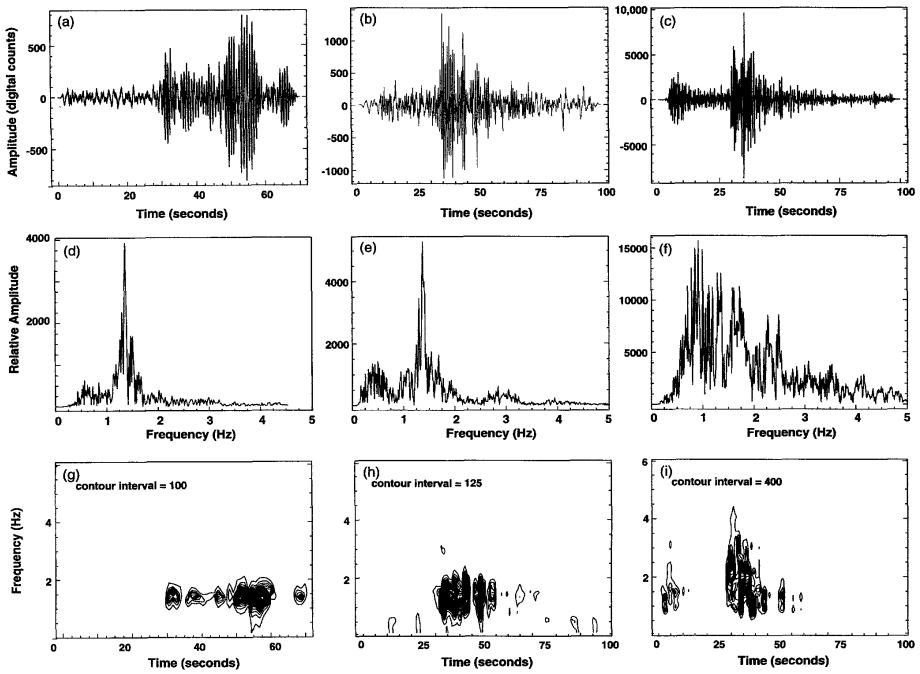


**Figure 31: Comparison of seismograms a) a seismic event associated with calving of a tidewater glacier in Prince William Sound, Alaska, b) glacier-generated event in the Mt. Ogden area and c) seismic event near Mt. Ogden (Wolf et al., 1997).**

It is clear from the seismograms of glacier earthquakes (Figure 31a and b) that the NE-trend events have different seismic characteristics are much more similar to the periodic

seismicity near Mt. Ogden on the Alaska-British Columbia border (Figure 31c) the frequency-magnitude relationship for a typical swarm that occurred during May 1996, with magnitudes greater than 2.2, gives a *b*-value of 1.0, which is similar to the *b*-value of the NE-trend. Both the Steele Glacier and Kluane Glacier were not surging in the last year and have not been for some time (G. Clarke, personal communication, 23 March 2012). Thus, it is unlikely that the NE-trend events are glacier earthquakes.

Finally, I briefly consider whether the NE-trend events result from changes in the hydrologic cycle. It has been suggested that the Mt. Ogden swarm was caused by transient changes of the pre-existing stress regime, resulting from variations in pore pressure due to changes in surface loading or to increased surface water input in the hydrologic cycle (Wolf et al., 1997). However, most of the NE-trend events are deeper than would be expected for earthquakes triggered by changes in the hydrologic cycle on a time scale of a few months. As well, it is probably unrealistic for pore pressure changes on a short time scale to cause weakness at depths greater than 10 km.

In conclusion, the NE-trend has a tectonic source based on seismic characteristics, *b*-values that are similar to those of tectonic events, and alignment along a fault.

## 4.6 Frequency-Magnitude Statistics for Southwest Yukon

Frequency-magnitude statistics were calculated for the Duke River Fault, NE-trend, and the northern and southern Denali Fault clusters (Figure 9). *b*-values and *a*-values for three different time periods were assessed for each of the four clusters (Table 5; refer to Appendix A for corresponding incremental and cumulative frequency-magnitude plots).

There are not enough events (<20) to calculate *b*-values for the northern and southern Denali Fault segments between September and November 2010.

**Table 5: Frequency-magnitude statistics for Duke River Fault, NE-trend, and northern and southern Denali Fault segments for three time periods.**

| Region | Jan.1985-Aug.2010 | Jan.1985-Nov.2011 | Sept.2010-Nov.2010 |
|---|---|---|---|
| Duke River Fault | b= 0.889 +- 0.078<br>a= 2.712 +- 0.199 | b= 0.881 +- 0.070<br>a= 2.681 +- 0.172 | b= 0.854 +- 0.152<br>a= 0.922 +- 0.174 |
| NE-trend | b= 0.941 +- 0.181<br>a= 2.003 +- 0.425 | b= 1.110 +- 0.181<br>a= 2.564 +- 0.424 | b= 0.961 +- 0.145<br>a= 1.476 +- 0.210 |
| Northern Denali Fault | b= 0.915 +- 0.115<br>a= 1.975 +- 0.224 | b= 0.924 +- 0.115<br>a= 1.989 +- 0.225 | |
| Southern Denali Fault | b= 0.846 +- 0.075<br>a= 2.430 +- 0.176 | b= 0.864 +- 0.075<br>a= 2.487 +- 0.176 | |

Over the longest time period, January 1985 to November 2011, the *b*-value is highest for the NE-trend (*b*=1.10) and lowest for the southern Denali Fault (*b*=0.864). There is greater uncertainty in the *b*-value for the NE-trend because of smaller range of magnitude events. The NE-trend only has events smaller than M<4. This may also be an indication why the NE-trend has a higher *b*-value, since a greater number of smaller events correspond to higher *b*-values and overall lower ambient stress in the region.

Prior to the YUK array, the *b*-value for the NE-trend was lower (0.941 +- 0.181) and more similar to that of the Duke River Fault (0.889±0.07). Additionally, the northern and southern segments of the Denali Fault have similar *b*-values (0.9) to those of the Duke

River Fault. The NE-trend has comparable *b*-values to other faults in southwest Yukon suggesting that the NE-trend events are tectonic.

The only previous low-level monitoring in the St. Elias Region was conducted by Horner (1983) between September 1978 and March 1981. He identified the Denali Fault as one of two principle zones of seismicity. The northern Denali Fault between 1985 to 2011 (Table 5) has a very similar recurrence curve of 0.924±0.115 to the low-level monitoring of the Denali Fault over a 39 month interval of 0.82±0.05. This is also comparable to the one based on historical record of 0.9±0.08 (Horner, 1983). The similar recurrence curve for the periods from January 1985 to November 2011, and September 1978 to March 1981, has a comparable minimum magnitude of completeness of 2.0. Additionally, a 5 week micro-seismic survey over 40 km of the Denali Fault indicate depths less than about 15 km (Horner, 1983). This coincides well with free depths observed around the central Denali Fault Yukon between September 2010 and November 2011 of less than 15 km (Figure 23).

## 4.7 Frequency-Magnitude Statistics Before and After the 2002 M=7.9 Denali Fault Earthquake

The 3 November 2002 M7.9 Denali Fault earthquake was one of the largest inland earthquakes in North America in the past 150 years (Ruppert, 2008) (Figure 32). It had a total rupture length of ~330 km and over 35,000 aftershocks by the end of 2004. On 23 October prior to the mainshock, there was a M6.7 event, the "Nenana Mountain" earthquake. There were over 1,000 detected aftershocks following the 23 October event (Ruppert, 2008). Changes in the probability of earthquakes caused by large earthquakes

in the vicinity, may be estimated by changes in *a* and *b*-values in the frequency-magnitude recurrence relation (Wiemer & Wyss, 2002). By permanent we are referring to the duration comparable to the catalogue length available since the event.

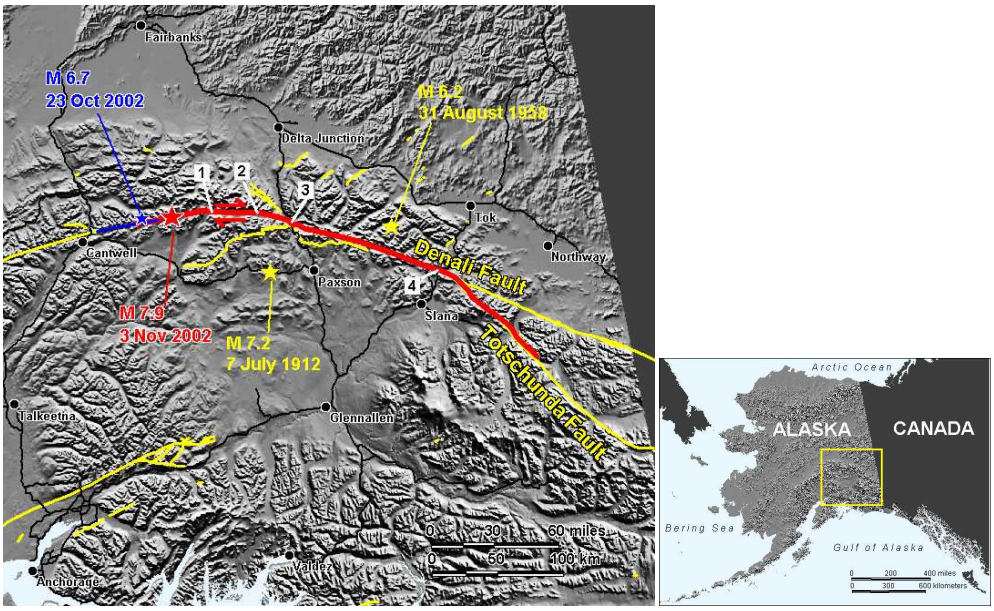


**Figure 32: Map of the Alaska portion of the Denali Fault showing the epicentre of 2002 Denali Fault earthquake (red star). The blue star represents the preceding M6.7 23 October earthquake, and yellow stars are other large shallow earthquakes in the vicinity of the fault. The red line shows the rupture length after the M7.9 Denali Fault earthquake (Combellick, 2009).**

Prior to the 1992 M7.3 Landers earthquake in California the Coulomb stress increased by 1 bar at the epicentre before rupture due to four M>5 earthquakes within 50 km of its epicentre. The four moderate earthquakes may have advanced the Landers earthquake by 100-300 years (King et al., 1994). Because high *b*-values are associated with low ambient stress, the Landers earthquake decreased the overall ambient stress, even though in some areas the Coulomb criterion increased the probability of failure, thus causing more

smaller earthquakes and higher *b*-values. On average, there were more areas where earthquake production increased, thus on average higher *b*-values, resulting in more frequent small earthquakes after the Landers earthquake (Wyss & Wiemer, 2000).

Earthquakes from January 1985 to November 2002 on the northern segment of the Denali Fault Yukon before the 2002 M7.9 Denali earthquake give a *b*-value of 0.81 ± 0.14 and an *a*-value of 1.52 ± 0.14. After the 2002 Denali earthquake, from November 2002 to December 2011, the *b*-value increased to 1.05 ± 0.22 and the *a*-value to 1.87 ± 0.45. Uncertainties in the *b*-values are larger than usual due to the low number of events (~25-50) and small magnitude range of events. As in the case of the 1992 Landers earthquake, the *b*-value increased after the 2002 Denali event, although caution is warranted because the uncertainties are comparable to the change in *b*-value. The increase in average *b*-value suggests that the northern segment of the Denali Fault had higher Coulomb stress after the 2002 earthquake (Wiemer & Wyss, 2002). The average local magnitude prior to the 2002 Denali earthquake was ~2.4, whereas the average magnitude afterward was ~1.9, which indicates that more frequent smaller earthquakes are triggered after the mainshock than before. The increased *b*-value and increase Coulomb stress suggest that the probability of failure along the fault has increased (Wyss & Wiemer, 2000). In 2011 there seems to be a seismic quiescence of the northern segment of the Denali Fault in the Yukon.

# Chapter 5: Conclusion

## 5.1 Summary

The main objective of this thesis was to provide a better understanding of the relationship between the micro-seismicity and tectonics in the southwest Yukon, Canada. I focused on four clusters of earthquakes to identify how the new denser YUK array has improved earthquake locations and depths, to identify active structures based on events located using the Progressive Multiple Event Location (PMEL) algorithm, and to evaluate rates of seismicity.

The addition of the YUK array allowed smaller events to be located and resulted in the detection of a NE-trend cluster of seismicity. As well, there is a high concentration of seismicity around the Duke River Fault and in a region parallel to the Alaska-Yukon border between the Duke River Fault and northern Denali Fault. The minimum magnitude of completeness for the southwest Yukon seismicity decreased from M3.0 to M1.0, improving frequency-magnitude statistics and seismic hazard analysis. Between September 2010 and November 2011, event magnitudes range from 0.2 to 4.7 and depths from 0 to 35 km.

In summary, three different station geometries were considered for earthquake locations: 1) CNSN data only; 2) CNSN data and YUK array data; and 3) CNSN data with both YUK and 3) CNSN data with both YUK and Alaska data. When YUK stations were included with the original CNSN network for events along the Duke River Fault and NE-trend, locations shift ~7 km to the southwest. However, this is likely due to an inappropriate detailed earth model and a bias in station distribution, as all YUK stations

are located to the northeast of the Duke River Fault and NE-trend. The most accurate locations are observed when the AEIC network is combined with the original CNSN network and YUK array. This yields a good azimuthal station distribution and some close-in stations. Combining the AEIC network with the CNSN network, events within the NE-trend show an average shift of ~6.6 km to the northeast and an average decrease in depth of 2.6 km. This suggest that original catalogue locations using only CNSN data are reasonably well-located, that solutions using only CNSN and YUK array are likely mislocated about 7 km to the southwest, and the best locations are those that include both YUK data and Alaska data. For the latter situation, events within the Duke River and NE-trend clusters have an average maximum horizontal error of ±0.9 km and an average error in depth of ±3.2 km.

Use of the Progressive Multiple Event Location (PMEL) technique on the Duke River and NE-trend events shows that the events fall along the Duke River Fault and the NE-trend events lie along or very near to map surface faults. The average global rms error for the *pmelavg* locations is ±0.07 s, in contrast to an average rms error of ±0.4 s for the single event locations of the combined CNSN and AEIC networks. The NE-trend has a length of 12.4 km with an azimuth of ~18°.

An important result of improved earthquake locations is the determination of free depths. There are 179 free depths in southwest Yukon. Free depths of events in the Duke River and NE-trend clusters range from 0 to 20 km with an average depth of 10.88 km. These depths are not well-constrained, as the closest stations are at distances of more than 20 km. Within the southern Denali Fault cluster there are two events with well-

constrained depths at distance less than ~8 km from station YUK6, with depths of 4.8 km and 8.2 km, consistent with an upper crust (2-10 km) focal depths.

One of the most significant results of this study was the detection of the NE-trend. The sources of these events suggests transfer of stress inland from the Yakutat block region. Studies suggest that deformation in the northern Cordillera is dominated by the broad effects of the Yakutat collision and that this collision is the cause of different regions of seismicity in the southwest Yukon. The belt of earthquakes around the Duke River Fault region and the events within the NE-trend are likely examples of seismicity due to the transfer of stress inland (Leonard et al., 2007).

I calculated frequency-magnitude statistics for each of the four clusters. *b*-values range from ~0.8 to ~1.1. Changes in *b*-values were calculated along the northern Denali Fault segment in the Yukon before and after the M7.9 2002 Denali Fault earthquake. *b*-values increased from 0.81 ± 0.14 to 1.05 ± 0.22, which indicates more frequent smaller earthquakes and hence a higher Coulomb stress.

The improved detection of smaller events in southwest Yukon as a result of the YUK array and more accurate locations and depths of these events important to better understand the tectonics and rates of seismicity in the Yukon. This will be useful information for the infrastructure and route planning of the Alaska pipeline.

## 5.2 Future Considerations

The relatively short period of about 15 months of data on which this study was based limits some of the results in this thesis. To identify the source of the NE-trend events, more data (time) will be necessary. Depth also needs to be better constrained to determine more conclusively the source of these events. Another seismic station closer to the NE cluster will be necessary to determine how many of these depths are in fact greater than 10 km. If depths are greater than 10 km, we can definitively rule out shallow ice- or glacier-related seismicity or water-induced seismicity. More data will also improve frequency-magnitude statistics of each cluster and variations in *b*-values before and after a mainshock. With five or more years of data, we will be able to determine the change in *b*-values before and after the deployment of the YUK array.

# References

Bilich, A., Cassidy, J., & Larson, K. (2008). GPS seismology: Application to the 2002 M 7.9 Denali Fault earthqauke. *Bulletin of Seismological Society of America,* 101, 2662-2674.

Billings, S., Sambridge, M., & Kennett, B. (1994). Errors in hypocenter location: picking, model, and magnitude dependence. *Bulletin of Seismological Society of America,* 84, 1878-1990.

Bridges, D., & Gao, S. (2006). Spatial variation of seismic b-values beneath Makushin Volcano, Unalaska Island, Alaska. *Earth and Planetary Science Letters,* 245, 408-415.

Bufe, C. (2006). Coulomb stress tranasfer and tectonic loading preceding the 2002 Denali Fault earthquake. *Bulletin of Seismological Society of America,* 96, 1662-1667.

Cassidy, J., Rogers, G., & Ristau, J. (2005). Seismicity in the vicinity of the SNORCLE corriders of the northern Canadian Cordillera. *Canadian Journal of Earth Sci*ences, 42, 1137-1148.

Combellick, R. (2009). Denali Fault earthquake M7.9 November 3, 2002. http://www.nichols.edu/departments/physicalworld/Denali%20Fault%20Earthquake.htm

Cornell, C., & Vanmarcke, E. (1969). The major influences on seismic risk. *Proceedings on the Fourth World Conference on Earthquake Engineering,* 1, 69-83.

Gulick, S., Lowe, L., Pavlis, T., Gardner, J., & Mayer, L. (2007). Geophysical insights into the transition fault debate: propagating strike slip in response to stalling Yakutat Block subduction in the Gulf of Alaska. *The Geological Society of America*, 35, 763-768.

Gutenberg, B., & Richter, C. (1944). Frequency of Earthqaukes in California. *Journal of the Seismological of Society of America,* 34, 185-188.

Hamburger, M., Shoemaker, K., Horton, S., DeShon, H., Withers, M., Pavlis, G., et al. (2011). Aftershocks of the 2008 Mt Carmel, Illinois, earthquake: evidence for conjugate faulting near the termination of the Wabash Valley fault system. *Seismological Research Letters,* 82, 735-747.

Havskov, J., & Ottemoller, L. (2010). *Routine data processing in earthquake seismology.* New York: Springer, 380, 116-123

Helmstetter, A., Kagan, Y. Y., & Jackson, D. D. (2008). Importance of small earthquakes for stress transfers and earthquake triggering. *Journal of Geophysical Research,* 116, B03312.

Horner, R. (1983). Seismicity in the St. Elias region of northwestern Canada and southeaastern Alaska. *Bulletin of the Seismological Society of America,* 73, 1117-1137.

Husen, S., & Hardebeck, J. (2010). Earthquake location accuracy. *Community Online Resource for Statistical Analysis, doi:10.5078/*corssa-55815573.

Hyndman, R., Fluck, P., Mazzotti, S., Lewis, T., Ristau, J., & Leonard, L. (2005). Current tectonics of the northern Canadian Cordillera. *Canadian Journal of Earth Sciences,* 42, 1117-1136.

Johnston, S. (2001). The great Alaskan terrane wreck: reconciliation of paleomagnetic and geological data in the northern Cordillera. *Earth and Planetary Science Letters,* 193, 259-272.

Johnston, S., & Canil, D. (2007). Crustal architecture of the SW Yukon, northern Cordillera: implications for crustal growth in a convergent margin orogen. *Tectonics,* 26, TC1006.

Kao, H., Shan, S.-J., Bent, A., Woodgold, C., Rogers, G., Cassidy, J. F., et al. (2011). Regional centroid-moment-tensor analysis for earthquake in Canada and adjacent regions: An Update. *Seismological Research Letters,* 83, 505-515.

Katsumata, K. (2006). Imaging the high b-value anomolies within the subducting Pacific plate in the Hokkaido corner. *Earth Planets Space,* 58, 49-52.

King, G., Stein, R., & LIn, J. (1994). Static stress changes and the triggering of earthquakes. *Bulletin of Seismological Society America,* 84*, 935-953.*

Lawrence, W., & Qamar, A. (1978). Hydraulic Transients: A seismic Source in Volcanoes and Glaciers. *Science,* 203, 654-656.

Leonard, L., Hyndman, R., Mazzotti, S., Nykolaishen, L., Schmidt, M., & Hippchen, S. (2007). Current deformation in the northern Canadian Cordillera inferred from GPS measurements. *Journal of Geophysical Research,* 112, B11401.

Leonard, L., Mazzotti, S., & Hyndman, R. (2008). Deformation rates estimated from earthquakes in the northern Cordillera of Canada and eastern Alaska. *Journal of Geological Research,* 113, B08406.

Lipovsky, P. S., Evans, S. G., Clague, J. J., Hopkinson, C., Couture, R., Bobrowsky, P., et al. (2008). The July 2007 rock and ice avalanches in Mount Steele, St. Elias Mountains, Yukon, Canada. *Spriner-Verlag,* 5, 445-455

Main, I., Irving, D., Musson, R., & Reading, A. (1999). Constraints on the frequency-magnitude relation and maximum magnitudes in the UK from observed seismicity and glacio-isostatic recovery rates. *Geophysical Journal International,* 137, 535-550.

Mazzotti, S., & Hyndman, R. (2002). Yakutat Collision and Strain Transfer across the Northern Canadaian Cordillera. *Geological Society of America,* 30*,* 495-498.

Mazzotti, S., Leonard, L., Hyndman, R., & Cassidy, J. (2008). Tectonics, dynamics and seismic hazard in the Canada-Alaska Cordillera. In *Active Tectonics and Seismic Potential of Alaska*. American Geophysical Union, 179, 297-319

Pacheco, J., Scholz, C., & Sykes, L. (1992). Changes in frequency-size relationship form small to large earthquakes. *Nature,* 355, 71-73.

Pavlis, G. (1983). *dbpmel*. Retrieved 2008 from Boulder Real Time Technologies: http://www.brtt.com/wiki/Dbpmel%281%29

Pavlis, G. (2008). *dbpmel*. From Boulder Real Time Technologies: http://www.brtt.com/wiki/Dbpmel%281%29

Pavlis, G. (2007). *pmelavg*. From Boulder Real Time Technologies: http://www.brtt.com/w/index.php?title=Pmelavg%281%29

Pavlis, G., & Booker, J. (1983). Progressive Multiple Event Location. *Bulliten of the Seismological Society of America*, 73, 1753-1777.

Power, M. (1988). Microearthquake seismicity on the Duke River, Denali Fault system. *Exploration and Geological Services Division*, 61-68.

Quinlan, D., & Pavlis, G. (2007). *Boulder Real Time Technologies*. From dbgenloc: http://www.brtt.com/w/index.php?title=Dbgenloc%281%29

Ratchkovski, N. (2003). Change in stress directions along the central Denali Fault, Alaska after the 2002 earthquake sequencce. *Geophysical Research Letters*, 30, 2017.

Rhoades, D. (1996). Estimation of Gutenberg-Richter relation allowing for individual earthquake magnitude uncertainies. *Tectonophysics, 258*, 71-83.

Richards, P. G., WaldHauser, F., Schaff, D., & Kim, W.-Y. (2006). The Applicability of Modern Methods of Earthquake Location. *Pure and Applied Geophysics*, 163, 351-372.

Ruppert, N. (2008). *M=7.9 Denai Fault earthquake of November 3rd, 2002*. From AEIC Alaska Earthquake Information: http://www.aeic.alaska.edu/Denali_Fault_2002/

Rydelek, P., & Sacks, I. (1989). Testing the completeness of earthquake catalogs and the hypothesis of self-similarity. *Nature*, 337, 251-253.

Schorlemmer, D., & Wiemer, S. (2004). Earthquake statistics at Parkfield: 1.stationarity of b-values. *Journal of Geophysical Research,* 109, B12307.

Schorlemmer, D., Wiemer, S., & Wyss, M. (2005). Variation in earthquake-size distribution across different stress regimes. *Nature,* 437, 539-542.

Shearer, P. (1997). Improving local earthquake locations using the L1 norm and waverform cross correlation: Application to the Whittier Narrows, California, aftershock sequence. *Journal Geophysical Reserarch*, 102, 8269-8284.

TransCanada. (2012). *About Us*. From Alaska Pipeline Project: http://thealaskapipelineproject.com/about_us

Tsai, V. C., Rice, J. R., & Fahnestock, M. (2008). Possible mecahnisms for glacial earthquakes. *Journal of Geophysical Research, 113*, 1-17.

Urbanic, T., Trifu, C.-I., Long, J., & Toung, R. (1992). Space-time correlation of b values with stress release. *Pure Applied Geophysics, 139*, 449-462.

USGS. (2010). *Focal Mechanisms*. From Earthquake Hazards Program: http://earthquake.usgs.gov/learn/topics/beachball.php

Waldhauser, F., & Ellsworth, W. (2000). A double-difference earthquake location algorithm: method and application to the northern Hayward Fault, California. *Bulletin of Seismolgical Society of America,* 90, 1353-1368.

Weichert, D. (1980). Estimation for earthquake recurrence parameters for unequal observation periods for different magnitudes. *Bulletin of Seismological Society of America, 70*, 1337-1346.

Wells, D., & Coppersmith, K. (1994). New empirical relationships among magnitude, rupture length, rupture width, rupture area and surface displacement. *Bulletin of Seismological Society of America,* 84, 974-1002.

Wiemer, S., & Wyss, M. (2002). Mapping spatial variability of the frequency-magnitude distribution of earthquakes. *Advances in Geophysics*, 45, 259-302

Woessner, J., & Wiemer, S. (2005). Assessing the quality of earthquake catalogues: estimating the magnitude of completeness and its uncertainty. *Bulletin of Seismological Society of America,* 95, 684-698.

Wolf, L., Rowe, C., & Horner, R. (1997). Periodic seismicisity near Mt. Ogden on the alaska-british columbia border: a case for hydrologically triggered earthquakes. *Bulletin of the Seismological Society of America*, 87, 1473-1483.

Wood, M. M. (2010). *"How do I locate that earthquake's epicenter"*. From UPSSeis an educational site for budding seismologists: http://www.geo.mtu.edu/UPSeis/locating.html

Wyss, M., & Wiemer, S. (2000). Change in the probability for earthquakes in Southerm California due to the Landers magnitude 7.3 earthquake. *Science*, 290, 1334-1338

# Appendix A

## B-Value Results

This appendix illustrates the statistics and results of the frequency-magnitude distribution for the Duke River Fault, NE-trending cluster, and the northern and southern Denali Fault segments.

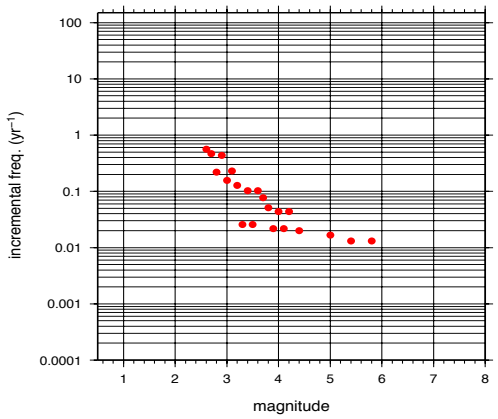


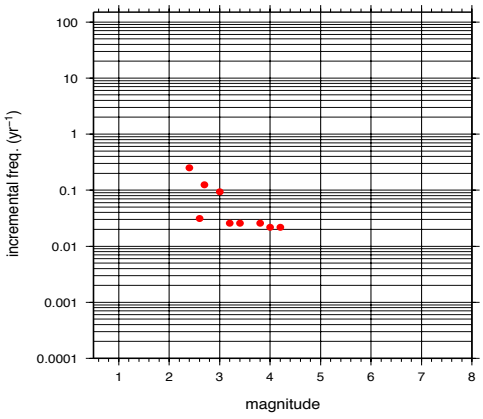


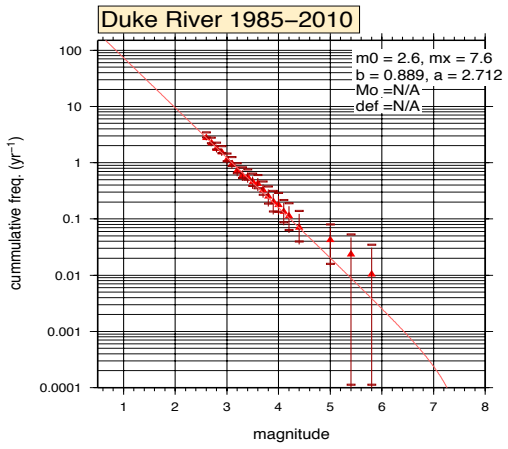


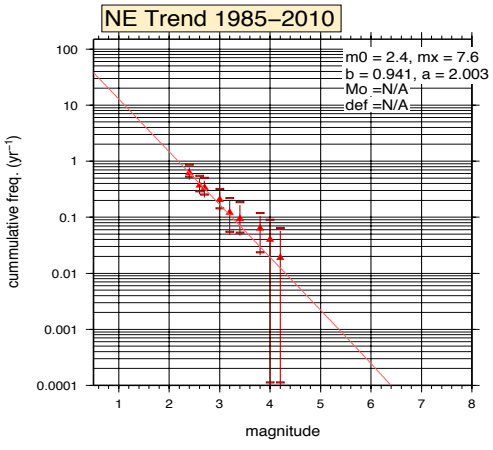

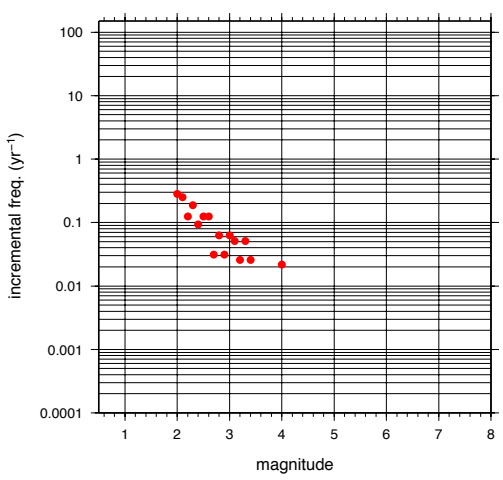
incremental freq. (yr⁻¹)
100
10
1
0.1
0.01
0.001
0.0001
1
2
3
4
5
6
7
8
magnitude

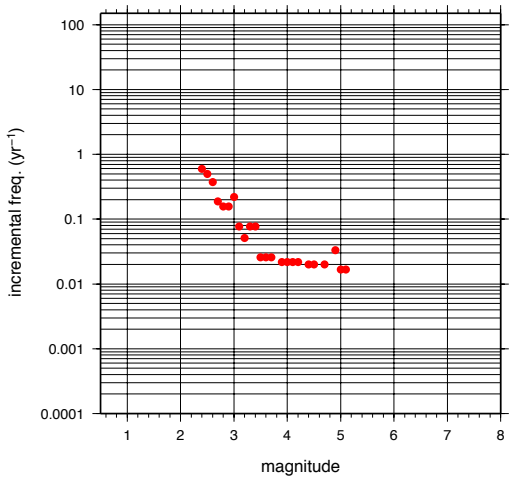
incremental freq. (yr⁻¹)
100
10
1
0.1
0.01
0.001
0.0001
1
2
3
4
5
6
7
8
magnitude

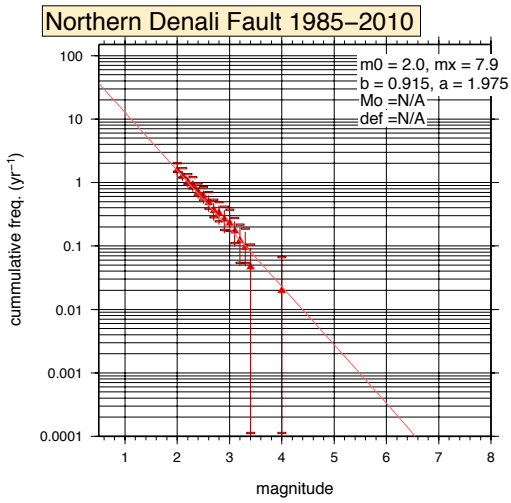
Northern Denali Fault 1985–2010
m0 = 2.0, mx = 7.9
b = 0.915, a = 1.975
Mo =N/A
def =N/A
cummulative freq. (yr⁻¹)
100
10
1
0.1
0.01
0.001
0.0001
1
2
3
4
5
6
7
8
magnitude

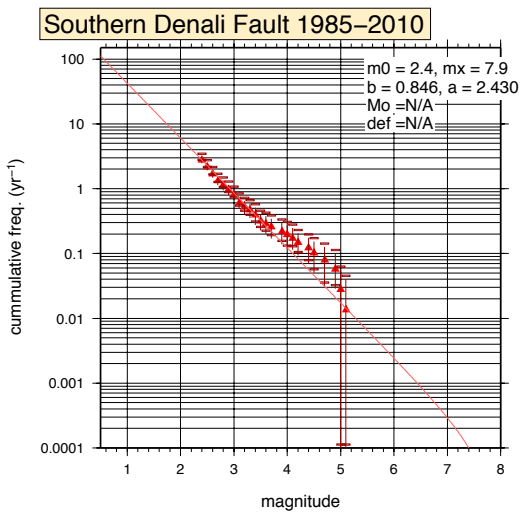
Southern Denali Fault 1985–2010
m0 = 2.4, mx = 7.9
b = 0.846, a = 2.430
Mo =N/A
def =N/A
cummulative freq. (yr⁻¹)
100
10
1
0.1
0.01
0.001
0.0001
1
2
3
4
5
6
7
8
magnitude

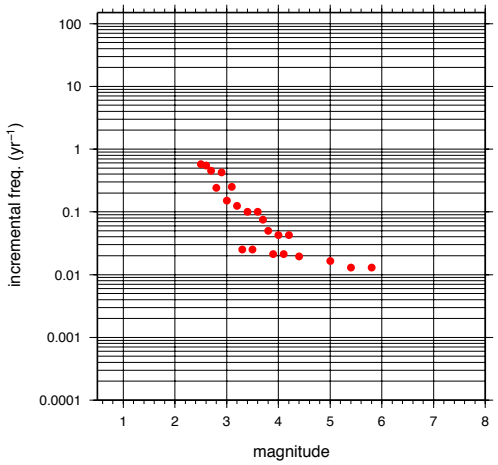
incremental freq. (yr⁻¹)
100
10
1
0.1
0.01
0.001
0.0001
1 2 3 4 5 6 7 8
magnitude

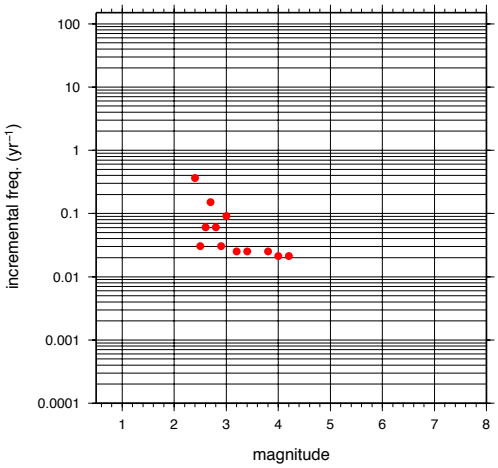
incremental freq. (yr⁻¹)
100
10
1
0.1
0.01
0.001
0.0001
1 2 3 4 5 6 7 8
magnitude

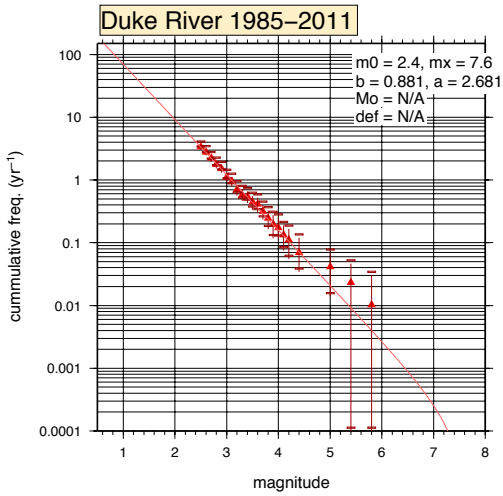
Duke River 1985–2011
m0 = 2.4, mx = 7.6
b = 0.881, a = 2.681
Mo = N/A
def = N/A
cummulative freq. (yr⁻¹)
100
10
1
0.1
0.01
0.001
0.0001
1 2 3 4 5 6 7 8
magnitude

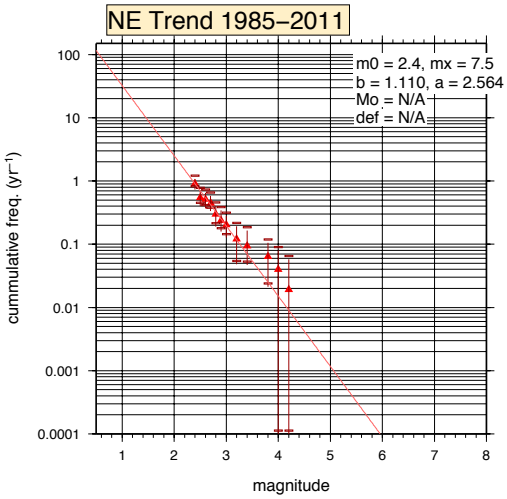
NE Trend 1985–2011
m0 = 2.4, mx = 7.5
b = 1.110, a = 2.564
Mo = N/A
def = N/A
cummulative freq. (yr⁻¹)
100
10
1
0.1
0.01
0.001
0.0001
1 2 3 4 5 6 7 8
magnitude

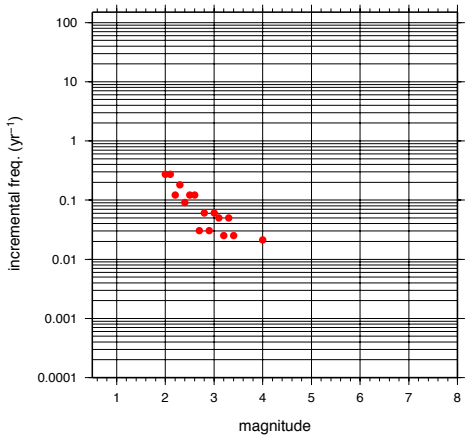
incremental freq. (yr⁻¹)
100
10
1
0.1
0.01
0.001
0.0001
1 2 3 4 5 6 7 8
magnitude

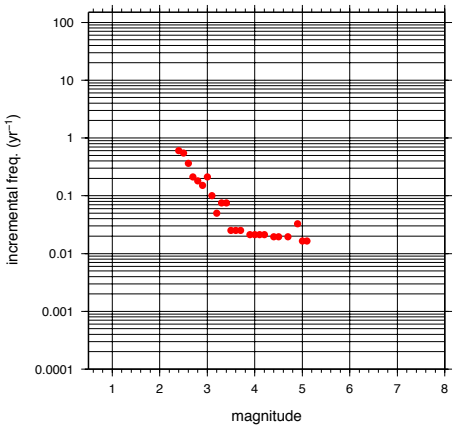
incremental freq. (yr⁻¹)
100
10
1
0.1
0.01
0.001
0.0001
1 2 3 4 5 6 7 8
magnitude

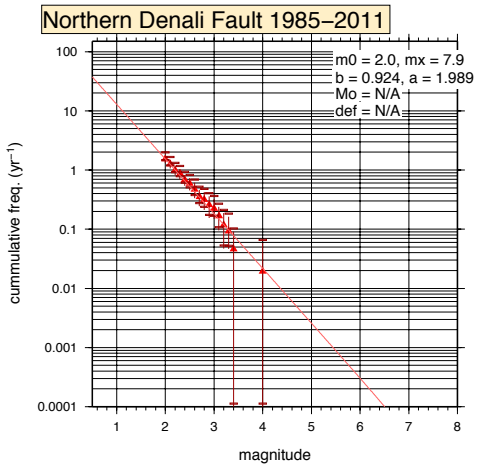
Northern Denali Fault 1985–2011
m0 = 2.0, mx = 7.9
b = 0.924, a = 1.989
Mo = N/A
def = N/A
cummulative freq. (yr⁻¹)
100
10
1
0.1
0.01
0.001
0.0001
1 2 3 4 5 6 7 8
magnitude

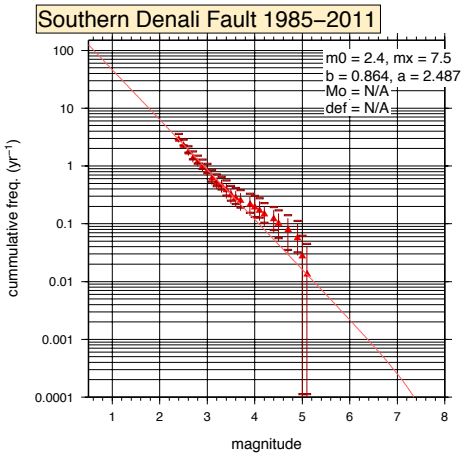
Southern Denali Fault 1985–2011
m0 = 2.4, mx = 7.5
b = 0.864, a = 2.487
Mo = N/A
def = N/A
cummulative freq. (yr⁻¹)
100
10
1
0.1
0.01
0.001
0.0001
1 2 3 4 5 6 7 8
magnitude

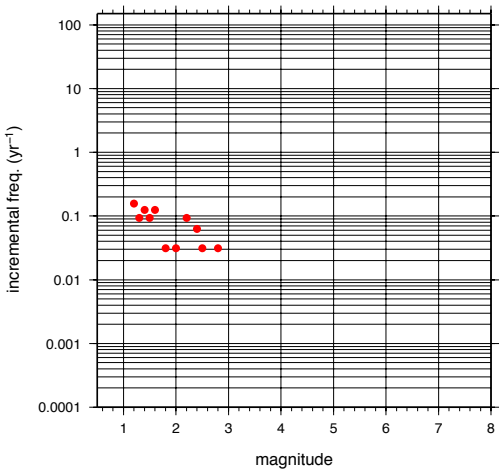
incremental freq. (yr⁻¹)
100
10
1
0.1
0.01
0.001
0.0001
1
2
3
4
5
6
7
8
magnitude

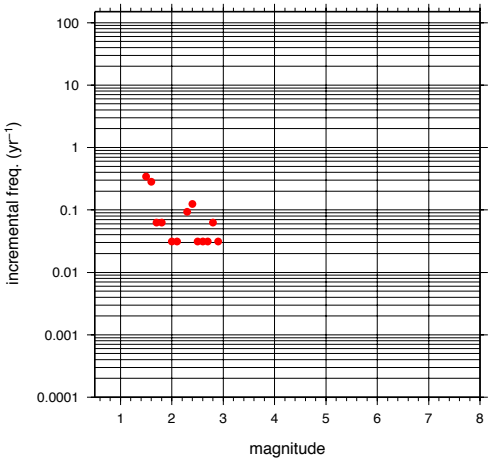
incremental freq. (yr⁻¹)
100
10
1
0.1
0.01
0.001
0.0001
1
2
3
4
5
6
7
8
magnitude

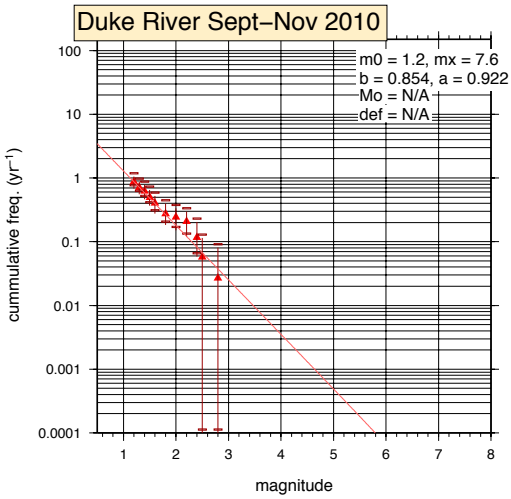
Duke River Sept–Nov 2010
m0 = 1.2, mx = 7.6
b = 0.854, a = 0.922
Mo = N/A
def = N/A
cummulative freq. (yr⁻¹)
100
10
1
0.1
0.01
0.001
0.0001
1
2
3
4
5
6
7
8
magnitude

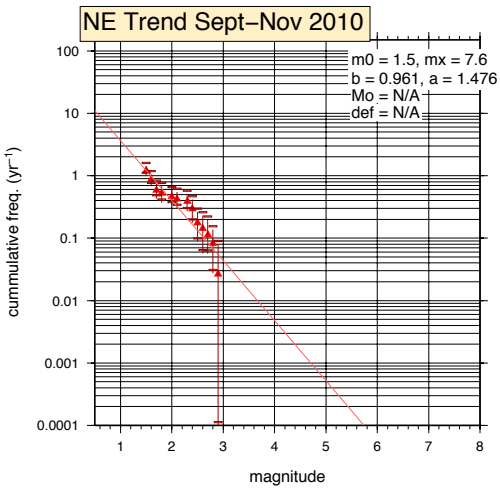
NE Trend Sept–Nov 2010
m0 = 1.5, mx = 7.6
b = 0.961, a = 1.476
Mo = N/A
def = N/A
cummulative freq. (yr⁻¹)
100
10
1
0.1
0.01
0.001
0.0001
1
2
3
4
5
6
7
8
magnitude

# Appendix B

Appendix B gives further details on some of the methods and further discussion of some of the results that was not included in the thesis.

## Progressive Multiple Event Location:

Hypocenter locations are estimated individually and their residuals are accumulated to estimate station corrections. Because earthquake locations are adjusted iteratively after each station correction adjustment, *dbpmel* promotes rapid convergence. Thus, its efficient usage of computer memory is one of the main advantages of using *dbpmel* over other relocation techniques.

The algorithm is performed by running four script files: 1) *makegclgrid* 2) *cluster* 3) *dbpmel* 4) *dbpmelavg.* First, a geographical curvilinear (GCL) grid is built called *makegclgrid* with control points on Earth's surface and at depths. For regional scale problems, this grid gives the best attempt to map a sphere onto a uniform grid. Each grid point has individual cylindrical grid cells with a specified maximum radius and depth range using an appropriate scale based on the density of hypocenters. Second, we construct a program called *cluster* that builds a simple cluster of events based on initial locations. The cluster searches in a cylindrical cell area until a minimum specified number of events are selected relative to each grid point. The events within the grid system create a new relational database that are sorted according to phase, control point, station and event. (Hamburger, et al., 2011) The *hypocentroid* table is created by the

*cluster* table. The two together define which events belong to a particular point in space. There are two parameters: *dlat*, *dlon* and *depth* define the control point of the grid while *hlat*, *hlon*, and *hdepth* define the location of hypocentroid. This is the centre of mass of the cluster associated with the control point (Pavlis, dbpmel, 1983). Third, *dbpmel* performs an iterative adjustment to provide revised locations and set of spatially variable station corrections. After running *dbpmel*, there will be an increase in event origins because the cylindrical cells around each control point overlap, thus one event may fall into several clusters, raising an issue of redundancy in event locations. Thus to solve this redundancy in arrival time estimates we take an average to produce one arrival time for each event and thus one event location.

This leads to the final step of running a program called *dbpmelavg.* This will give a final set of revised locations by averaging redundant locations. The averaging algorithm is a local or two joined algorithms, which can be used separately or combined together. In the local approach the location estimate is weighted by the reciprical of the root mean square (rms) residual, corresponding to *sdobs* in the *origerr* table. In the second approach, a distance dependent weighting is used. Each event within its cluster is compared to distance from its hypocenter of which it is associated. In the parameter file, a cutoff distance is set where an event is given full weight. If the distance between the event and the hypocenter is larger than the cutoff distance then a weight of 1/r is given. This is normalized to have a unit weight at the cutoff distance. To make the cutoff distance a mean, choose the cutoff distance to be a large value. For a nearest neighbour estimate, make the cutoff distance small compared to the grid spacing. If both methods

are used, the result is the weighted sum determined by multiplying the weights of the two terms together (Pavlis, pmelavg, 2007).

The error scale used to define outliers is not determined independently for each event as it is for single locations using *dbgenloc*, but rather the global rms of each cluster of events. This should give a more stable result since by definition global rms has more degrees of freedom than the rms of a single event. There are six parameters that handle outliers; three of these parameters handle the error scale: *pmel_initial_error_scale*, *pmel_minimum_error_scale* and *pmel_minimum_ sswrodgf*. *pmel_initial_error_scale* is the initial error when the rms statistics are not available. The other two parameters are used to prevent a downward spiral of continuous down weighting until all weights reduce to zero (Pavlis, dbpmel, 1983).

## Source of the NE-trend:

Since there is similarity in seismic characteristics of the NE-trending events to the earthquakes of the Mt. Ogden swarm, we consider that these events may be hydrologically triggered. However, most of the NE-trending events had depths that were deeper than one would expect for earthquakes triggered by changes in the hydrologic cycle or elevated or altered pore pressures influencing local stress regimes on a short term scale of a few months. Although the depths are not well-constrained, station distances are 20 or more km and events are less than 20 km, thus this is unlikely a major factor in determining the source of these earthquakes.

We also explore the possible explanation of induced or triggered failure due to surface loading or transient modifications to pre-existing stress regimes. Short term failure is probably related to the rate of loading or the combination between increased stress and undrained increases in pore pressure. Short term variations in pressures is unknown and may be linked to strained energy release triggering smaller magnitude earthquakes in the NE-trending cluster (Wolf, Rowe, & Horner, 1997) . However, if we consider the depths of the NE-trending events, it is probably unrealistic for pore pressure changes on a short term scale to cause zones of weakness at depths greater than 10 km. It is unclear whether the diffusive properties of the subsurface and depths are not well constrained, thus pore pressure variations cannot be ruled out completely. Short term variations in surface loading causing transient changes to the pre-existing stress regime may be a plausible cause of the NE-trending events.

We also investigated the possibility that a few of these events within the NE-trend may be triggered by landslides, induced by ice avalanches. There was a major ice avalanche at Mt. Steele in July, 2007. This was one of 18 large rock avalanches known to have occurred since 1899 on the slopes adjacent to glaciers in northwestern Canada (Lipovsky, et al., 2008). At least three rock and ice avalanches occurred between July 22$^{nd}$, 2007 and July 24$^{th}$, 2007. Seismographs in Alaska and the Yukon recorded the July 22$^{nd}$ ice avalanche at a local magnitude of 2.1. Due to the large difference in body and surface wave magnitudes, it was recognized as a mass movement rather than an earthquake. The main event occurred on July 24$^{th}$ at 1757 hours local time and recorded at a local magnitude of 3.4. We compared the seismic characteristics of the main event of the ice

avalanche to two events in the NE-trend around the time of July 24th, 2007 at the common station HYT and also to events within the NE-trend during Sept. and Oct. 2010 at station HYT. Similarities in the waveforms may be an indication during Sept. and Oct. 2010 of seismic activity triggered by landslides.

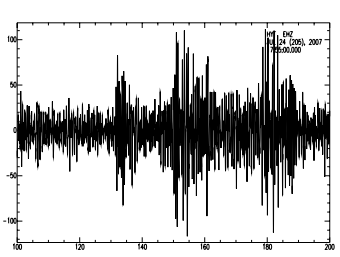

**Figure 33a: HYT HHZ of mainevent July 24th, 2007.**

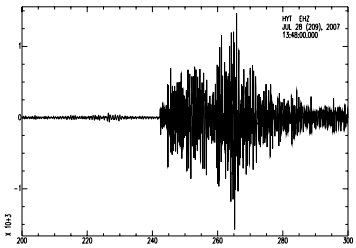

**Figure 26b: HYT HHZ NE event July 28th, 2007.**

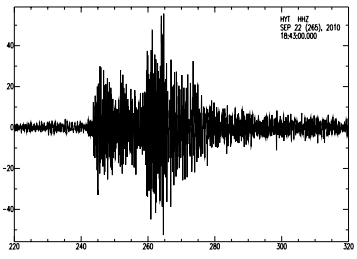

**Figure 26c: HYT HHZ NE event Sept. 22nd, 2010.**

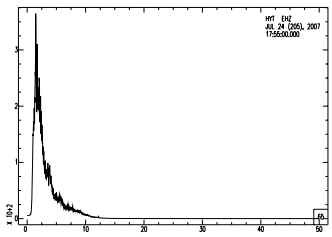

**Figure 26d: frequency spectrum July 24th, 2007.**

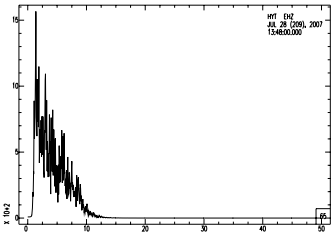

**Figure 26e: frequency spectrum July 28th, 2007.**

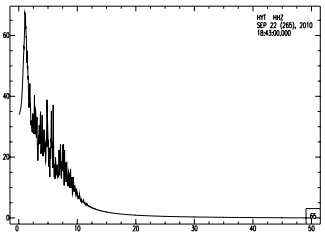

**Figure 26f: frequency spectrum Sept. 22nd 2010.**

The July 24th ice avalanche caused an event that was very noisy or very emergent P and S arrivals and therefore hard to distinguish these arrivals. The NE-trending events on July 28th, 2007 and September 22nd, 2010, had similar emergent P and S arrivals and dominant frequencies of ~1 Hz that decrease rapidly. The two NE-trending events had smaller magnitudes of 1.6 and 1.9 compared to the magnitude 3.4 of the ice avalanche and thus variations in amplitude and frequency. Although the frequency spectrums are similar, landslides due to ice avalanches may be a trigger for a few of the events in the NE-trend but not significant in the overall source of earthquakes of the NE-trend.

# Appendix C

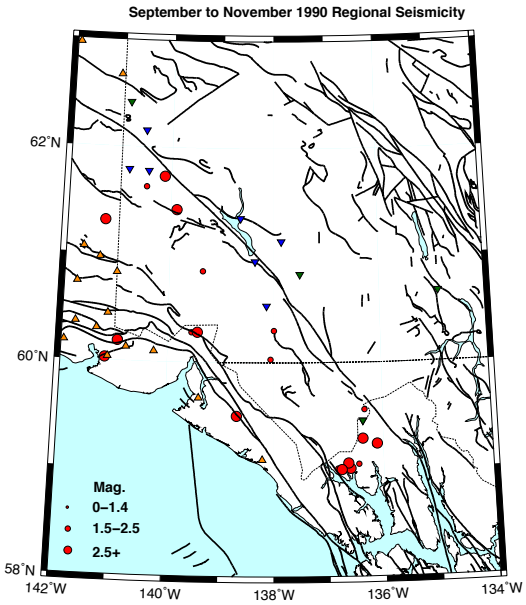
September to November 1990 Regional Seismicity
62°N
60°N
58°N
142°W
140°W
138°W
136°W
134°W
Mag.
0–1.4
1.5–2.5
2.5+

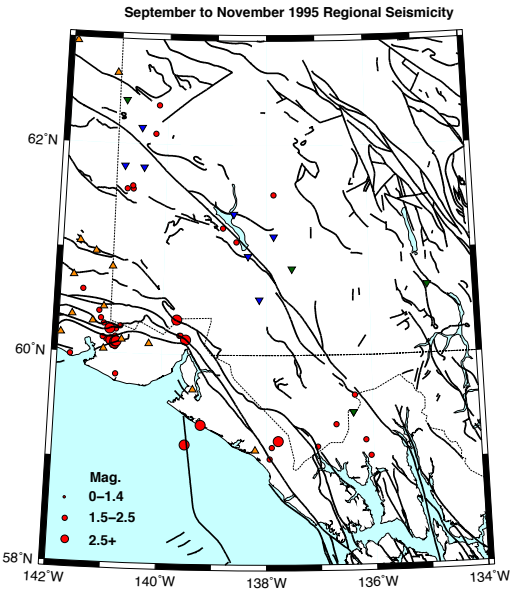
September to November 1995 Regional Seismicity
62°N
60°N
58°N
142°W
140°W
138°W
136°W
134°W
Mag.
0–1.4
1.5–2.5
2.5+

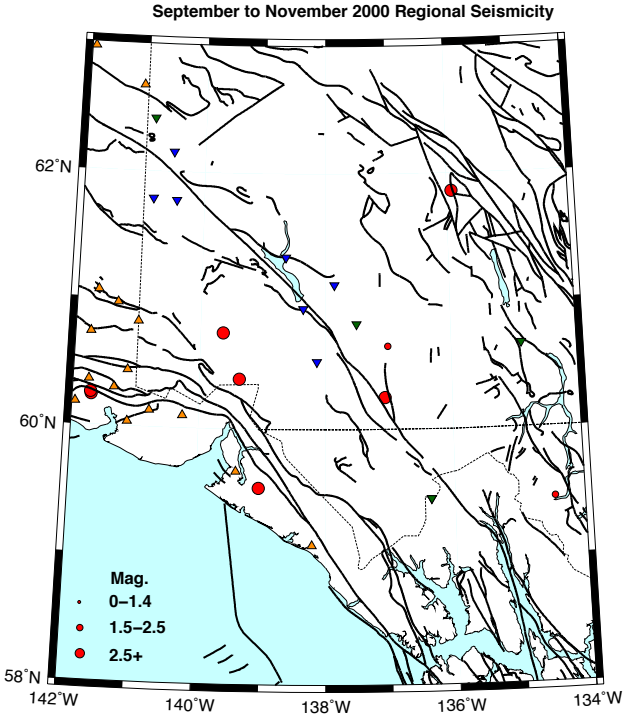
September to November 2000 Regional Seismicity
62°N
60°N
58°N
142°W
140°W
138°W
136°W
134°W
Mag.
0–1.4
1.5–2.5
2.5+